Neurobiology of Disease

Compartmentalized Regulation of Parkin-Mediated Mitochondrial Quality Control in the *Drosophila* Nervous System *In Vivo*

Hyun Sung, Lauren C. Tandarich, Kenny Nguyen, and Peter J. Hollenbeck
Department of Biological Sciences, Purdue University, West Lafayette, Indiana 47907

In neurons, the normal distribution and selective removal of mitochondria are considered essential for maintaining the functions of the large asymmetric cell and its diverse compartments. Parkin, a E3 ubiquitin ligase associated with familial Parkinson's disease, has been implicated in mitochondrial dynamics and removal in cells including neurons. However, it is not clear how Parkin functions in mitochondrial turnover *in vivo*, or whether Parkin-dependent events of the mitochondrial life cycle occur in all neuronal compartments. Here, using the live *Drosophila* nervous system, we investigated the involvement of Parkin in mitochondrial dynamics, distribution, morphology, and removal. Contrary to our expectations, we found that Parkin-deficient animals do not accumulate senescent mitochondria in their motor axons or neuromuscular junctions; instead, they contain far fewer axonal mitochondria, and these displayed normal motility behavior, morphology, and metabolic state. However, the loss of Parkin did produce abnormal tubular and reticular mitochondria restricted to the motor cell bodies. In addition, in contrast to drug-treated, immortalized cells *in vitro*, mature motor neurons rarely displayed Parkin-dependent mitophagy. These data indicate that the cell body is the focus of Parkin-dependent mitochondrial quality control in neurons, and argue that a selection process allows only healthy mitochondria to pass from cell bodies to axons, perhaps to limit the impact of mitochondrial dysfunction.

Key words: autophagy; axonal transport; *Drosophila*; mitochondria; mitophagy; Parkin

Significance Statement

Parkin has been proposed to police mitochondrial fidelity by binding to dysfunctional mitochondria via PTEN (phosphatase and tensin homolog)-induced putative kinase 1 (PINK1) and targeting them for autophagic degradation. However, it is unknown whether and how the PINK1/Parkin pathway regulates the mitochondrial life cycle in neurons *in vivo*. Using *Drosophila* motor neurons, we show that *parkin* disruption generates an abnormal mitochondrial network in cell bodies *in vivo* and reduces the number of axonal mitochondria without producing any defects in their axonal transport, morphology, or metabolic state. Furthermore, while cultured neurons display Parkin-dependent axonal mitophagy, we find this is vanishingly rare *in vivo* under normal physiological conditions. Thus, both the spatial distribution and mechanism of mitochondrial quality control *in vivo* differ substantially from those observed *in vitro*.

Introduction

Neurons are large, morphologically asymmetric and functionally compartmentalized cells. For this reason, they rely critically on robust, organized axonal transport to maintain the normal distribution of organelles among the somatodendritic, axonal, and synaptic compartments (Hirokawa et al., 2010; Saxton and Hollenbeck, 2012). Mitochondria play an important role in neuronal function and survival, as they supply ATP, buffer cytosolic calcium, and generate reactive oxygen species, and thus their transport and redistribution within neurons are particularly important (Saxton and Hollenbeck, 2012). They display a unique and complex life cycle that is characterized by bidirectional movement (Stowers et al., 2002; Guo et al., 2005; Glater et al., 2006; Pilling et al., 2006; Reis et al., 2009), morphological changes

Received Feb. 26, 2016; revised April 7, 2016; accepted May 18, 2016.

Author contributions: H.S. and P.J.H. designed research; H.S. performed research; H.S., L.C.T., and K.N. analyzed data; H.S. and P.J.H. wrote the paper.

This work was supported by National Institutes of Health/National Institute of Neurological Disorders and Stroke Grant 5R01-NS-027073. We thank L.J. Pallanck (University of Washington, Seattle, WA) for providing flies (*D42-Gal4>UAS-mitoGFP*), (*park*^{25}, *D42-Gal4/TM6B*), (*park*^{25}, *UAS-mitoGFP/TM6B*), and (*UAS-Parkin/Cy0*); E. Hafen (ETH, Zürich, Switzerland) for providing flies (*UAS-RFPatg8/Cy0*); J.C. Clemens (Purdue University, West Lafayette, IN) for providing anti-HRP; and Elisabeth Garland-Kuntz for assisting with blinded analysis of mitochondrial morphology.

The authors declare no competing financial interests.

Correspondence should be addressed to Peter J. Hollenbeck, Department of Biological Sciences, Purdue University, 915 West State Street, West Lafayette, IN 47907. E-mail: phollenb@purdue.edu.

DOI:10.1523/JNEUROSCI.0633-16.2016
 0270-6474/16/367375-17$15.00/0

(Okamoto and Shaw, 2005; Chan, 2006; Song et al., 2009), and complex biogenesis and degradation (Davis and Clayton, 1996; Amiri and Hollenbeck, 2008; Maday et al., 2012; Ashrafi et al., 2014). In neurons, these components of the mitochondrial life cycle are closely interrelated: for example, the dysregulation of mitochondrial axonal transport can affect organelle morphology (Pathak et al., 2010), while altered fission–fusion balance can impair axonal mitochondrial motility (Verstreken et al., 2005; Baloh et al., 2007; Misko et al., 2010; Yu et al., 2016). Although it has been thought that the neuronal lysosomal compartment resides mainly near the nucleus, the presence, transport, and development of late endosomes (Deinhardt et al., 2006) and lysosomes (Moughamian and Holzbaur, 2012) have been demonstrated in axons. Additionally, in axons, local biogenesis (Amiri and Hollenbeck, 2008), fission–fusion (Cagalinec et al., 2013), and turnover (Maday et al., 2012; Ashrafi et al., 2014) of mitochondria are reported to occur. Thus, the regulation of the mitochondrial life cycle and the maintenance of a robust functional population, collectively termed mitochondrial "quality control" (QC; Chen and Chan, 2009; Rugarli and Langer, 2012), are likely to be more complex in neurons *in vivo* than in cells of more modest dimensions due to the potential distribution of functions among distant compartments.

It has been proposed that mitochondrial dynamics and QC are functionally regulated by two Parkinson's disease-related genes, PTEN (phosphatase and tensin homolog)-induced putative kinase 1 (PINK1) and the E3 ubiquitin ligase Parkin. Recent data from *Drosophila* suggest that PINK1/Parkin catalyze mitochondrial arrest by tagging for degradation of the mitochondria–kinesin linker protein Miro (Wang et al., 2011; Liu et al., 2012), and also prevent the fusion of senescent mitochondria with healthy ones by downregulating the mitochondrial fusion protein Mitofusin 2 (Deng et al., 2008; Poole et al., 2008, 2010). Furthermore, studies in non-neuronal cells indicate that PINK1 and Parkin target depolarized, dysfunctional mitochondria for autophagic engulfment and degradation (Narendra et al., 2008, 2010; Matsuda et al., 2010; Ashrafi et al., 2014; Lazarou et al., 2015). Although the question of whether this pathway governs mitochondrial QC in all neuronal compartments remains unsolved, these findings suggest that PINK1 and Parkin may cooperate in the maintenance of neuronal mitochondrial distribution and function by regulating mitochondrial dynamics and turnover.

Here, we used the intact *Drosophila* larval nervous system for *in vivo* study, complemented by cultured larval primary neurons as an *in vitro* system, to analyze the life cycle of neuronal mitochondria. We assessed the following three processes: mitochondrial axonal transport, fission–fusion, and degradation. We found that the loss of Parkin diminishes axonal mitochondrial flux without disturbing most features of movement. In addition, although Parkin-deficient motor neurons displayed greatly reduced numbers of axonal mitochondria, their organelle morphology and membrane potential were normal. However, mitochondrial morphology was disrupted in cell bodies, suggesting that this compartment houses Parkin-dependent QC *in vivo*. We also observed a striking difference in the extent of axonal mitophagy between *in vitro* motor neurons, where it was abundant, and the same neurons *in vivo*, where it was rare. Together, these observations indicate that Parkin-dependent mitochondrial QC differs significantly in location and abundance between *in vivo* and *in vitro* systems, and further suggest that Parkin regulates mitochondrial axonal access *in vivo*.

Materials and Methods

Drosophila *strains and culture conditions.* All flies were reared on standard cornmeal agar medium and maintained at 25°C with a 12 h light/dark cycle. The GAL4-UAS system was used to visualize mitochondria, and autophagosomes specifically, in motor neurons. Wild-type flies expressing a single copy of mitochondrially targeted GFP (mito-GFP) or coexpressing mito-GFP with RFP-Atg8 driven by *D42* driver were used as the controls (*w; +/+; D42-Gal4>UAS-mitoGFP/+*) and (*w; UAS-RFPatg8/UAS-RFPatg8; D42-Gal4>UAS-mitoGFP/+*; Pilling et al., 2006). Parkin-null mutants, (*w; +/+; park^{25}, D42-Gal4/park^{25}, UAS-mitoGFP*) and (*w; UAS-RFPatg8/UAS-RFPatg8; park^{25}, D42-Gal4/park^{25}, UAS-mitoGFP*), were used in this study (Greene et al., 2003). Genetically overexpressed Parkin in the null mutant background, (*w; UAS-Parkin/+; park^{25}, D42-Gal4/park^{25}, UAS-mitoGFP*), was used for rescue experiments. For starvation conditions, third instar larvae were collected and maintained in a distilled water-moisturized dish without food for 6 h.

Dissected larval preparation for observing neuronal mitochondria in vivo. To image mitochondria in live motor neurons, late third instar larvae were collected, dissected, and prepared as previously described (Devireddy et al., 2014). In brief, larvae were pinned ventral side down on a Sylgard plate and dissected with a handheld scissors (catalog #15000-00, Fine Science Tools) from posterior to anterior along the dorsal body wall in HL6 buffer containing 0.6 mM $CaCl_2$ and 4 mM[SCAP] L-glutamate. Fat bodies and intestine were then removed to reveal the intact ventral ganglion (VG), segmental nerves (SNs), and neuromuscular junctions (NMJs; Pilling et al., 2006; Louie et al., 2008; Shidara and Hollenbeck, 2010). The dissected larva was then placed dorsal side up on a glass slide and covered by a glass coverslip using dental wax as a spacer to form a chamber. This was filled with HL6 buffer and sealed with Valap for imaging. Mitochondria in both cell bodies and axons of larval motor neurons were observed using laser-scanning confocal microscopy (LSCM; C1 on an Eclipse 90i microscope, Nikon) within 20 min of dissection to ensure normal *in vivo* conditions of the nervous system (Shidara and Hollenbeck, 2010; Devireddy et al., 2014).

Time-lapse microscopy for organelle axonal transport analysis. To analyze axonal transport of organelle in motor neurons, time-lapse images of mito-GFP and RFP-Atg8 were acquired from the longest SN in the following three different regions: proximal (segment A2); middle (segment A4); and distal (segment A7) to the VG. Time-lapse confocal images were obtained using 5% laser power with a 488 nm band for mito-GFP and 10% laser power with a 561 nm band for RFP-Atg8 through the smallest pinhole (30 μm). The region imaged was 50 μm in length, and frames for individual channels (513/30 for mito-GFP and 590/50 for RFP-Atg8) were obtained at 1 s time intervals for 2 min. The following parameters of transport were quantified essentially as previously described by the manual tracking function of ImageJ software (Devireddy et al., 2014). Briefly, mitochondrial and autophagosomal flux were measured for both anterograde and retrograde movement by observing the number of moving organelles passing a defined point per unit time over 2 min. Since some diffuse RFP-Atg8 signals were seen throughout the cytosol, only vacuoles above a threshold intensity (1000 on a 12 bit scale) were designated as autophagic vacuoles (AVs). Mitochondrial velocity was measured from continuous mitochondrial movements of $>$3 s duration in one direction. One pixel represents 0.1 μm in our confocal images, and only net velocities of $>$0.1 μm/s or < -0.1 μm/s for at least three consecutive frames were selected as bona fide anterograde and retrograde transport, respectively. During 2 min time-lapse movies, only mitochondria that moved for $>$60 s were considered for velocity analysis. Mitochondrial moving and stationary percentage was measured from the total population of mitochondria within a field. Since the population of mitochondria within the assigned axonal regions included a changing set of moving mitochondria, the second frame of each movie was selected for designating mitochondrial total population. Mitochondria in the population were categorized and marked as anterograde, retrograde, or stationary by ImageJ/Cell Counter to quantify the percentage of moving and stationary mitochondria in segmental axons. The mitochondrial duty cycle was measured for moving mitochondria by observing their movement or pause time over the observation interval. The percentage of the time that

mitochondria moved in each particular direction or paused was quantified, and again only mitochondria that moved for >60 s were considered for duty cycles. Mitochondrial run length was defined as the distance per individual run between stops. Mitochondrial net runs in the dominant direction only for both anterograde and retrograde movement were used for the run length measurement. Mitochondrial flux with photobleaching was measured from 50 μm regional length of middle (segment A4) SNs with 30 μm photo bleached for 30 s with full intensity of 488 nm light from the confocal laser. Time course images were acquired at a rate of 1 frame every 2 s for 5 min. Every 30 s, the number of steady-state moving mitochondria was quantified from the bleached regions. An exponential series was applied to estimate the number of steady-state moving mitochondria in bleached regions. Thirty and 29 steady-state moving mitochondria were estimated in control and *park*^{25}, *Parkin* animals respectively, while 17 steady-state moving mitochondria were estimated in *park*^{25} mutants from the 30 μm photo-bleached regions, as follows: control from ($y = 0.033e^{63.612x}$), *park*^{25} from ($y = 0.059e^{58.643x}$), and *park*^{25}, *Parkin* from ($y = 0.035e^{63.741x}$). These estimated numbers were nearly consistent with the numbers calculated from the percentage of moving mitochondria, as follows: ~27 steady-state moving mitochondria were calculated in controls, while ~16 steady-state moving mitochondria were calculated in *park*^{25} mutants from the bleached regions (data not shown).

Determination of organelle density and colocalization. MetaMorph version 7.6.5 software was used to measure the mitochondrial density in SNs based on the intensity of the mito-GFP signal (Devireddy et al., 2014). The second frame of each movie was selected, and the number of pixels with GFP signal above threshold was used to determine the density of mitochondria in the region of observation. To clarify the shape of the mitochondrial boundary, the selected frames of confocal images are converted to binary images with 400 minimum-intensity thresholds on a 12 bit scale of 0–4095. Mitochondrial density in NMJs was measured by NIS-Elements AR 3.2 software to analyze the area. In each NMJ, the polygonal ROI tool was used to draw the region around the synaptic boutons, and the area that was covered by mitochondria was calculated with the total area. A 515/30 (mito-GFP) channel was used for measuring mitochondrial density, whereas a 590/50 (anti-HRP) channel was used for measuring the area of synaptic boutons. The images were converted by representative thresholds (400 minimum intensity for mitochondria, and 200 minimum intensity for anti-HRP staining) to clarify the shape of the boundaries. Colocalization of AVs with mitochondria was quantified by NIS-Elements AR 3.2 software. The intensity profiles from two channels, 515/30 (mito-GFP) and 590/50 (RFP-Atg8), were used to analyze the colocalization in each region.

Immunostaining. For immunostaining of NMJs, late third instar larvae were partially dissected and fixed with 4% paraformaldehyde for 20 min at room temperature (Shidara and Hollenbeck, 2010). Fixed samples were washed with PBT (PBS containing 0.1% Triton X-100), and blocked with PBTB (PBT containing 0.2% BSA), then stained with mouse anti-HRP (1:1000) that was conjugated with Alexa Fluor 594 goat anti-mouse (a gift from J.C. Clemens, Purdue University, West Lafayette, IN). Immunostained samples were washed with PBTB before mounting and were observed by LSCM (C1 on an Eclipse 90i microscope, Nikon). Images of immunostained NMJs were taken between muscles 6 and 7 from A4 SNs.

Axonal mitochondria in adult fly wing. To observe axonal mitochondria in the wing nerve, 5-d-old adult flies were collected and paralyzed on a CO_2 anesthetizing pad. The fly wings were visualized under a dissection stereomicroscope and cut at the end of wing root to preserve a whole nerve tract along the humeral crossvein (HCV) with the first lateral vein (LV1) and costal vein of LV0 (Fang et al., 2012). Severed wings were pretreated with detergent (20%, Triton X-100 in dH_2O) to avoid trapping air bubbles, briefly rinsed with 1× PBS (Fang et al., 2013), placed dorsal side up on a glass slide, and covered by a glass coverslip using dental wax as a spacer. The chamber was filled by PBS and sealed with Valap for imaging. Images were taken using LSCM within 10 min to ensure normal *in vivo* conditions of the wing neuronal system. Axons of HCV from the wing arch were monitored to analyze axonal mitochondrial density. In all experiments, only the right wing from the female adult was used.

Morphological analysis of mitochondria. Image quantification was performed using NIS-Elements AR 3.2 software. Nonoverlapping axonal mitochondria from each SN (segment A2, segment A4, and segment A7) were selected for both length and area measurements, while in primary cultured neurons only length measurements were performed. Since 1 pixel represents 0.1 μm in the NIS-Elements AR 3.2 software images, the minimum standard distance unit was 0.1 μm. To determine the boundary of mitochondria for the length and area measurements, images were thresholded at a standard intensity of 200 to identify pixels belonging to mitochondria. Mitochondrial morphology in cell bodies was analyzed using both individual sections and three-dimensional image stacks. The latter were built from 20 μm (X, height) by 20 μm (Y, width) with 5 μm (Z, depth) of 100 z-stacks centered on the middle of the cell body. Morphological analyses were performed blinded to the experimental condition.

Measurement for mitochondrial membrane potential. Tetramethylrhodamine methyl ester (TMRM; Life Technologies), a lipophilic cationic fluorescent dye, was used for the determination of mitochondrial transmembrane potential both *in vivo* (Devireddy et al., 2014) and *in vitro* (Verburg and Hollenbeck, 2008). Thin neurons and NMJs adjacent to the middle SNs in larval A4 segment and projected axons of primary cells were selected for measuring neuronal mitochondrial membrane potential ($\Delta\Psi_m$) in *in vivo* and *in vitro* conditions, respectively. TMRM 200 nM in prepared medium (HL6 buffer or Schneider's medium) was added to the dissected larvae or cultured cells for 20 min, then replaced with 50 nM TMRM for imaging. Only nonoverlapping axonal mitochondria were considered for quantification. Images were obtained sequentially by 488 nm excitation with 5% laser power for mito-GFP and by 561 nm excitation with 5% laser power for TMRM. The ratio of mitochondrial fluorescence intensities (F_m) to cytoplasmic fluorescence intensities (F_c) was used to determine $\Delta\Psi_m$ (F_m/F_c; Verburg and Hollenbeck, 2008; Shidara and Hollenbeck, 2010; Devireddy et al., 2014).

Primary neuronal cell culture. Brain lobes and ventral ganglia were taken from third instar larvae and transferred into Schneider's medium. Tissue was incubated in 0.7 mg/ml collagenase for 1 h at room temperature and then dissociated to individual cells by siliconized pipette triturating. After dissociation, ~250 μl of cell solution was transferred to each glass coverslip in a cell culture dish and incubated for 1 h for cell adhesion. Glass coverslips were coated with 20 μg/ml concanavalin A for cell adhesion. Five to seven sets of CNS were used for two 35 mm cell culture dishes. After 1 h of incubation, 2 ml of Schneider's medium was added, and culture dishes were incubated for ~96 h to allow neurons to extend their processes. Antimycin A (Ant A; 5 μM) was treated for 20 min to depolarize mitochondria. For oxidative stress conditions, 100 μM H_2O_2 was added to the culture dishes 1 h before taking images.

Statistical analysis. To analyze data from *park*^{25} mutants compared with controls, p values were calculated using an unpaired homoscedastic t test. For multiple group comparisons, statistical significance was calculated by a one-way ANOVA with Bonferroni correction *post hoc* test. Significance between two populations was determined by two-sample Kolmogorov–Smirnov (K–S) test for analyzing the critical distribution. Correlations between two parameters were assessed by Pearson's correlation coefficient R^2 values. In all cases, at least three independent experiments were performed. All statistical significance was verified at $^*p < 0.05$, $^{**}p < 0.01$, and $^{***}p < 0.001$ using GraphPad Prism.

Results

Parkin loss affects axonal mitochondrial flux without disturbing most features of movement

The PINK1/Parkin pathway has been proposed both to support mitochondrial QC and turnover (Narendra et al., 2008, 2010; Matsuda et al., 2010), and to regulate mitochondrial motility (Wang et al., 2011; Liu et al., 2012; Saxton and Hollenbeck, 2012). These two functions are likely to be related, as the return of senescent mitochondria to the cell body would require targeted net retrograde traffic. Thus, one expectation is that Parkin deficiency

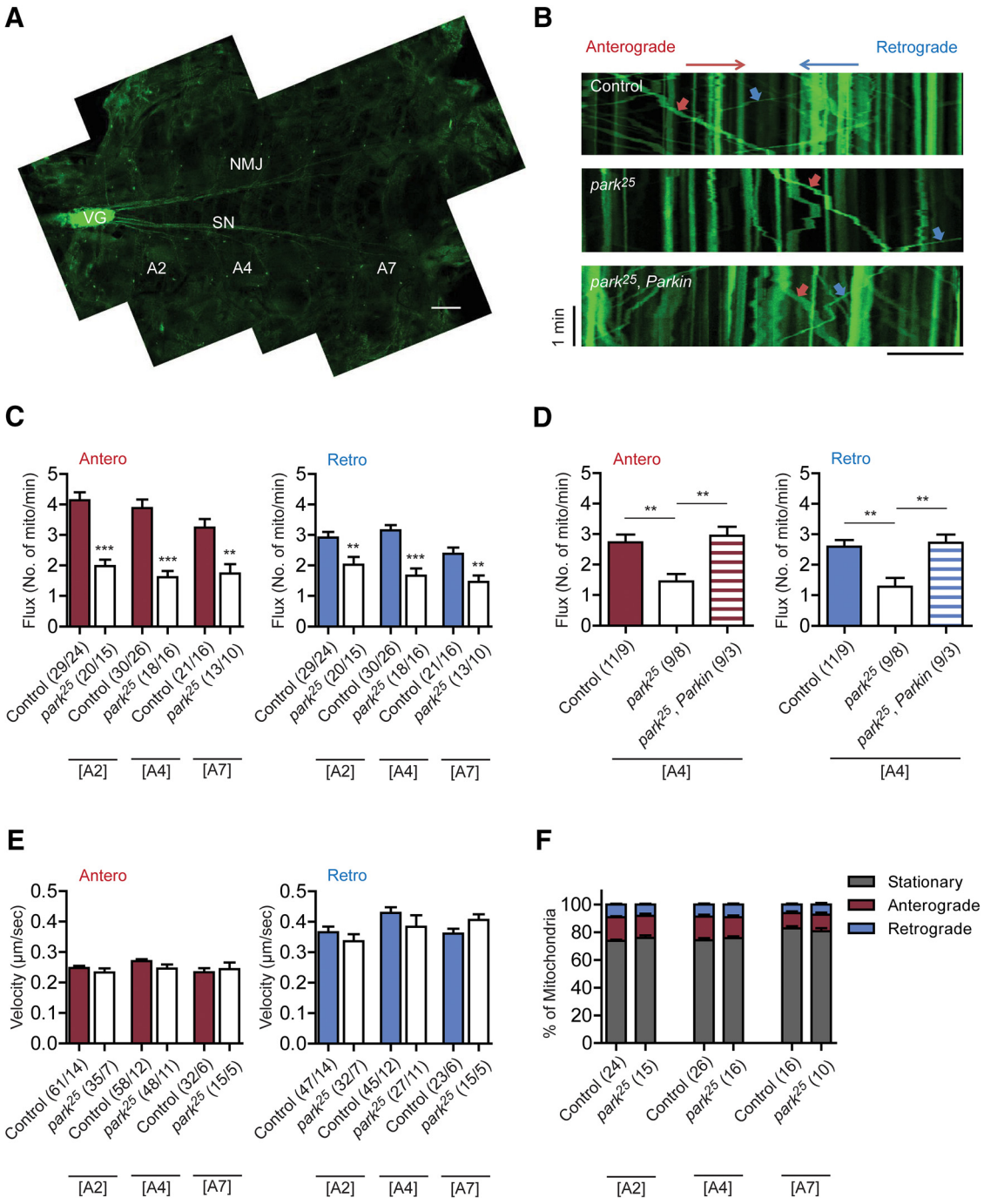

Figure 1. Parkin perturbation alters mitochondrial axonal traffic by reducing flux without affecting motility properties. ***A***, Confocal image of dissected late third instar larva expressing mito-GFP in motor neurons. Mitochondrial movements are monitored at three different regions in the axons of SNs: proximal (A2), middle (A4), and distal (A7). Thin branch nerves, adjacent NMJs, and cell bodies in the VG are also analyzed. Scale bar, 200 μm. ***B***, Representative kymographs of mitochondrial axonal transport from the A4 SNs. The red arrows indicate anterograde movements, while blue arrows indicate retrograde. Scale bar, 10 μm. ***C***, Mitochondrial flux in different *parkin* genotypes in A2, A4, and A7 SNs. *park*^{25} mutants display attenuated mitochondrial flux in both directions throughout SNs. (*n*/*n*), Number of axonal regions/number of animals. ***D***, Mitochondrial flux in *parkin* deletion and rescue in A4 SNs. The attenuated mitochondrial flux in *park*^{25} mutants is restored by *UAS-Parkin* expression. (*n*/*n*), Number of axonal regions/number of animals. ***E***, Mitochondrial net velocity in different *parkin* genotypes. *park*^{25} mutants show retain normal mitochondrial velocities in both directions throughout the SNs. (*n*/*n*), Number of mitochondria/number of animals. ***F***, The percentages of moving and stationary mitochondria are unaffected in *park*^{25} SNs. *n*, number of animals. Error bars indicate the mean ± SEM. Significance is determined by Student's *t* test (***C***, ***E***, and ***F***) or by one-way ANOVA with Bonferroni correction (***D***). $^{**}p < 0.01$ and $^{***}p < 0.001$.

will inhibit the turnover and/or retrograde traffic of mitochondria, causing an accumulation of senescent organelles in the axon. To test this hypothesis *in vivo*, we quantified the axonal transport of mitochondria in motor neurons of the intact *Drosophila* larval nervous system (Pilling et al., 2006; Russo et al., 2009). Using mito-GFP driven by *D42*, transport was quantified in both directions in the proximal (segment A2), middle (segment A4), and distal (segment A7) regions of the SNs, and was compared between control (wild-type with *D42-Gal4>UAS-mitoGFP*) and *park*^{25} (*parkin*-null) animals (Fig. 1*A*,*B*; Devireddy et al., 2014). Consistent with previous analysis, mitochondrial flux in control motor axons was greater in the anterograde than in the

Table 1. Duty cycle, run length, and area of axonal mitochondria from *Drosophila* larval motor neurons

	A2		A4		A7	
	Anterograde	Retrograde	Anterograde	Retrograde	Anterograde	Retrograde
Mitochondria duty cycle (% of time)						
Control						
S	46.45 ± 3.10	48.17 ± 2.94	36.03 ± 2.17	35.90 ± 2.16	38.57 ± 2.28	45.37 ± 3.97
A	51.83 ± 3.01	7.11 ± 1.24	60.46 ± 2.39	8.43 ± 1.36	60.26 ± 2.57	6.20 ± 1.39
R	1.73 ± 0.27	44.73 ± 2.50	3.52 ± 0.51	55.67 ± 2.53	1.17 ± 0.60	48.43 ± 5.01
Mitochondria (*n*)	61	47	58	45	32	23
park^{25}						
S	59.29 ± 3.37*	59.54 ± 3.50*	47.30 ± 3.89*	53.88 ± 5.80*	53.26 ± 4.97*	51.71 ± 6.61
A	39.83 ± 3.42*	4.26 ± 0.57	50.20 ± 3.88*	5.97 ± 0.97	45.44 ± 5.10*	4.21 ± 0.84
R	0.88 ± 0.31	36.20 ± 3.29*	2.50 ± 0.48	40.16 ± 5.39**	1.30 ± 0.47	44.08 ± 5.91
Mitochondria (*n*)	35	32	48	27	15	15
Mitochondria run length (μm)						
Control	2.44 ± 0.13	3.53 ± 0.35	3.08 ± 0.21	4.36 ± 0.33	2.96 ± 0.45	4.14 ± 0.53
Mitochondria (*n*)	61	47	58	45	32	23
park^{25}	2.37 ± 0.26	3.58 ± 0.44	2.98 ± 0.29	3.51 ± 0.20*	2.57 ± 0.19	3.73 ± 0.31
Mitochondria (*n*)	35	32	48	27	15	15
Mitochoncria area (μm^2)						
Control	0.81 ± 0.02		0.82 ± 0.01		0.82 ± 0.02	
Mitochondria (*n*)	151		204		177	
park^{25}	0.80 ± 0.01		0.79 ± 0.03		0.77 ± 0.02	
Mitochondria (*n*)	99		69		70	

Quantitative analysis of axonal mitochondrial duty cycle, run length, and area from control and *park*^{25} animals at three different regions of SNs (A2, A4, and A7). To define duty cycle, moving mitochondria are considered as the percentage of time spent in a specific direction: S, stationary; A, anterograde; or R, retrograde. Run length is defined from moving mitochondria, while area is measured from axonal mitochondria regardless of movement. Data were acquired from at least three independent experiments and are expressed as the mean ± SEM. *n*, Number of mitochondria. *$p < 0.05$ and **$p < 0.01$.

retrograde direction, and declined with distance from the cell body in SNs (Shidara and Hollenbeck, 2010). In *park*^{25} SNs, flux was attenuated in both directions (Fig. 1*C*). However, anterograde flux was more severely impaired than retrograde in *park*^{25} SNs: anterograde flux dropped to 48% (A2), 41% (A4), and 53% (A7) of control, while retrograde flux dropped to 70% (A2), 53% (A4), and 61% (A7). These deficits were rescued by Parkin overexpression in the null background (Fig. 1*B*,*D*).

Because this pathway has been proposed to specifically detach kinesin from the mitochondrial surface (Wang et al., 2011), we next examined whether reduced mitochondrial flux in *park*^{25} SNs derived from the alteration of particular elements of mitochondrial motility. We analyzed the mitochondrial velocities, percentage moving, duty cycle, and run length (Devireddy et al., 2014). In *park*^{25} SNs, mitochondrial velocities in both directions were similar to those of controls throughout the axons (Fig. 1*E*), and the percentages of moving and stationary mitochondria in motor axons were unaffected by Parkin deletion (Fig. 1*F*). This eliminated the major movement parameters as sources of the flux deficit, but we further measured the duty cycle and run length of moving mitochondria, and found that *park*^{25} mutants showed a modestly increased percentage of time pausing during mitochondrial movement in both directions, caused by the reduced proportion of movements in the dominant direction (Table 1). However, the run lengths of moving mitochondria were generally maintained with only a modest decrease in retrograde in the A4 region of SNs (dropped to 81%; Table 1). These data indicate that although the loss of Parkin significantly reduces mitochondrial flux in the axon, mitochondrial motility behaviors and the percentage of moving mitochondria are nearly unchanged.

Reduced mitochondrial flux in *park*^{25} motor axons results mainly from reduced organelle density

If mitochondrial motility was essentially normal in *park*^{25} mutants, what could explain the large decrease in flux? One possibility is that Parkin deficiency reduces the number of mitochondria in the axon. This would run contrary to expectations, since the proposed role of the PINK1/Parkin pathway in mitochondrial turnover predicts that Parkin deficiency would cause the accumulation of senescent mitochondria (Narendra et al., 2008, 2010; Matsuda et al., 2010). Nonetheless, we assessed this possibility by quantifying total mitochondrial density (both moving and stationary) in SN axons (Devireddy et al., 2014) and found that there was indeed a pronounced loss of axonal mitochondria throughout *park*^{25} motor axons, as follows: the mitochondrial densities in axons were reduced to 52% (A2), 61% (A4), and 56% (A7) of control levels in *park*^{25} SNs (Fig. 2*A*,*B*). This deficit was restored in A4 of *park*^{25} SNs by Parkin overexpression (Fig. 2*A*,*C*). To examine this deficit in *park*^{25} adult animals, we examined mitochondria in the wing, where a subset of sensory neurons expresses genes driven by *D42*, and these are situated along the wing margin (L0 vein and L1 vein) with L3 vein (Fang et al., 2012). We visualized *D42>mito-GFP* mitochondria in these sensory axons by observing the HCV of LV1 (Fig. 2*D*). As in the larval nervous system, HCV axons of *park*^{25} mutant wings showed reduced mitochondrial density; unlike the larval SNs, the deficit was not significantly restored by Parkin overexpression (Fig. 2*E*).

Because the majority of axonal mitochondria in SNs are persistently stationary (Fig. 1*F*), we assessed separately the density of the moving mitochondria. We photo bleached the mito-GFP in a 30 μm region of SN, quantified the entry of mitochondria into it over time in both directions (Fig. 3*A*), and extrapolated the densities to steady state using both linear and hyperbolic plots with good agreement (Fig. 3*B*,*C*). The *park*^{25} axons showed a density of moving mitochondria <60% that of controls, and this was partially rescued by Parkin overexpression. It was notable that, despite the lower densities of moving organelles, equal times were required to fill a bleached region to the steady state; both control and *park*^{25} animals required ~210 s to reach a plateau (Fig. 3*B*). This confirms the previous observations (Fig. 1) that the reduced mitochondrial flux seen in *park*^{25} SN axons results from reduced organelle density without significant changes in motility behavior.

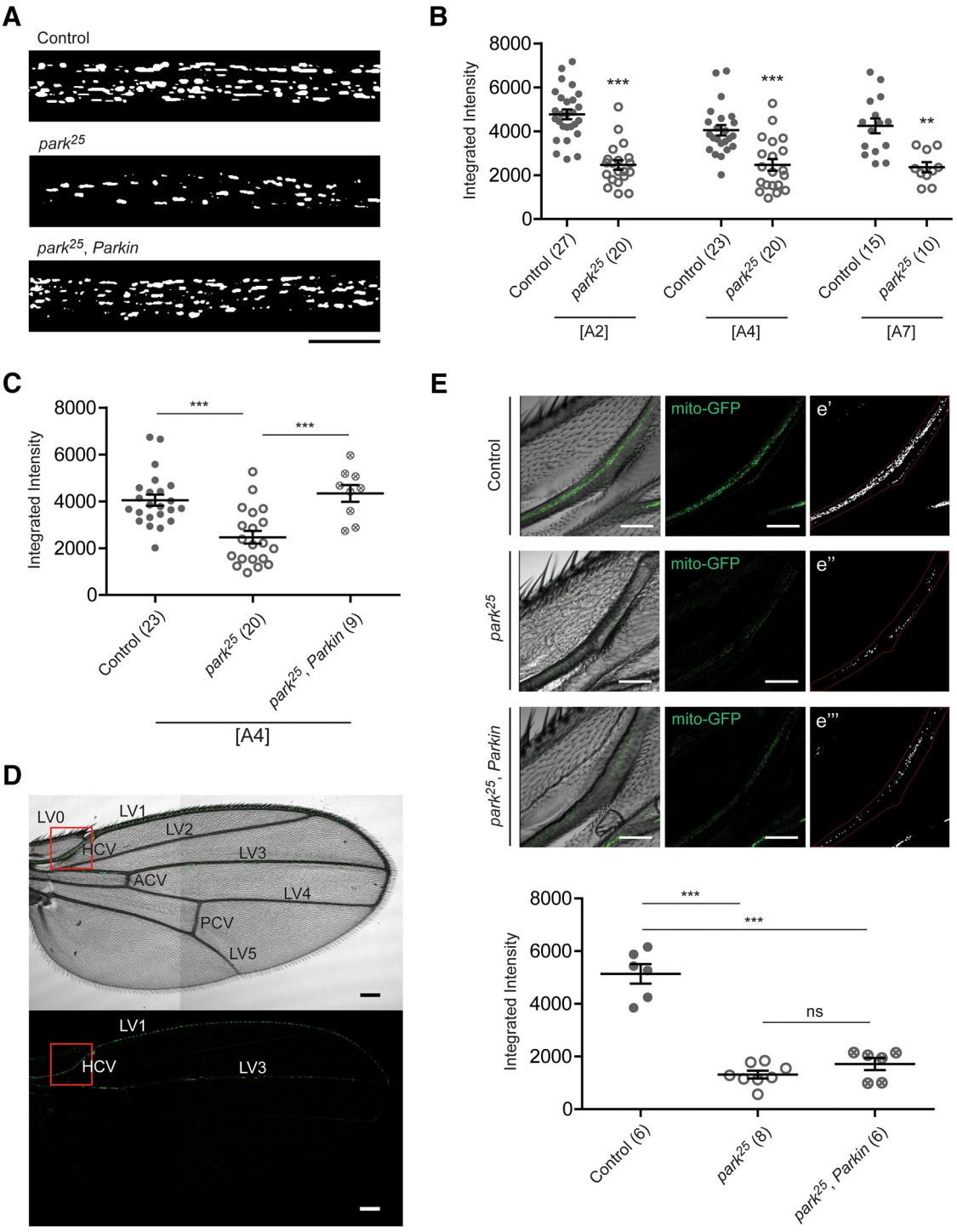

Figure 2. Reduced mitochondrial density is found in *park*^{25} motor axons. ***A***, Representative binarized images of mitochondria from the axon of A4 SNs. Scale bar, 10 μm. ***B***, Axonal mitochondrial density measurements from different *parkin* genotypes in the A2, A4, and A7 regions show that density is decreased by half in *park*^{25} mutants throughout the axons. ***C***, Axonal mitochondrial density from different *parkin* genotypes in A4 SNs shows that the decreased density in *park*^{25} axons is restored by *UAS-Parkin* expression. ***D***, Axonal mitochondria from 5-d-old adult fly wing. Axons from the HCV (red box) of the LV1 are monitored. Scale bars, 100 μm. ***E***, Axonal mitochondrial density in the HCV from different genotypes. Binarized images of mitochondria from the outlined area (***e'***, ***e''***, and ***e'''***) are quantified, and *park*^{25} mutants display reduced mitochondrial density in HCV. The deficit is not restored by *UAS-Parkin* expression in adult HCV. Scale bars, 50 μm. *n*, number of animals. Error bars indicate the mean ± SEM. Significance is determined by Student's *t* test (***B***) or by one-way ANOVA with Bonferroni correction (***C***, ***E***). $^{**}p < 0.01$ and $^{***}p < 0.001$.

Parkin mutation affects neither gross morphology nor $\Delta\Psi_m$ of axonal mitochondria

The Parkin pathway has also been proposed to keep senescent, depolarized mitochondria from fusing with normal ones by promoting the degradation of Mitofusin (Deng et al., 2008; Poole et al., 2010; Ziviani et al., 2010). Thus, another prediction is that *park*^{25} mutants will display longer mitochondria with diminished inner $\Delta\Psi_m$. To test this hypothesis, we first quantified the length of both stationary and moving axonal mitochondria, and found that neither was affected by *parkin* perturbation (Fig. 4*A*). Stationary mitochondria measured 1.54 ± 0.01 μm in controls versus 1.55 ± 0.01 μm in *park*^{25} mutants, while moving mito-

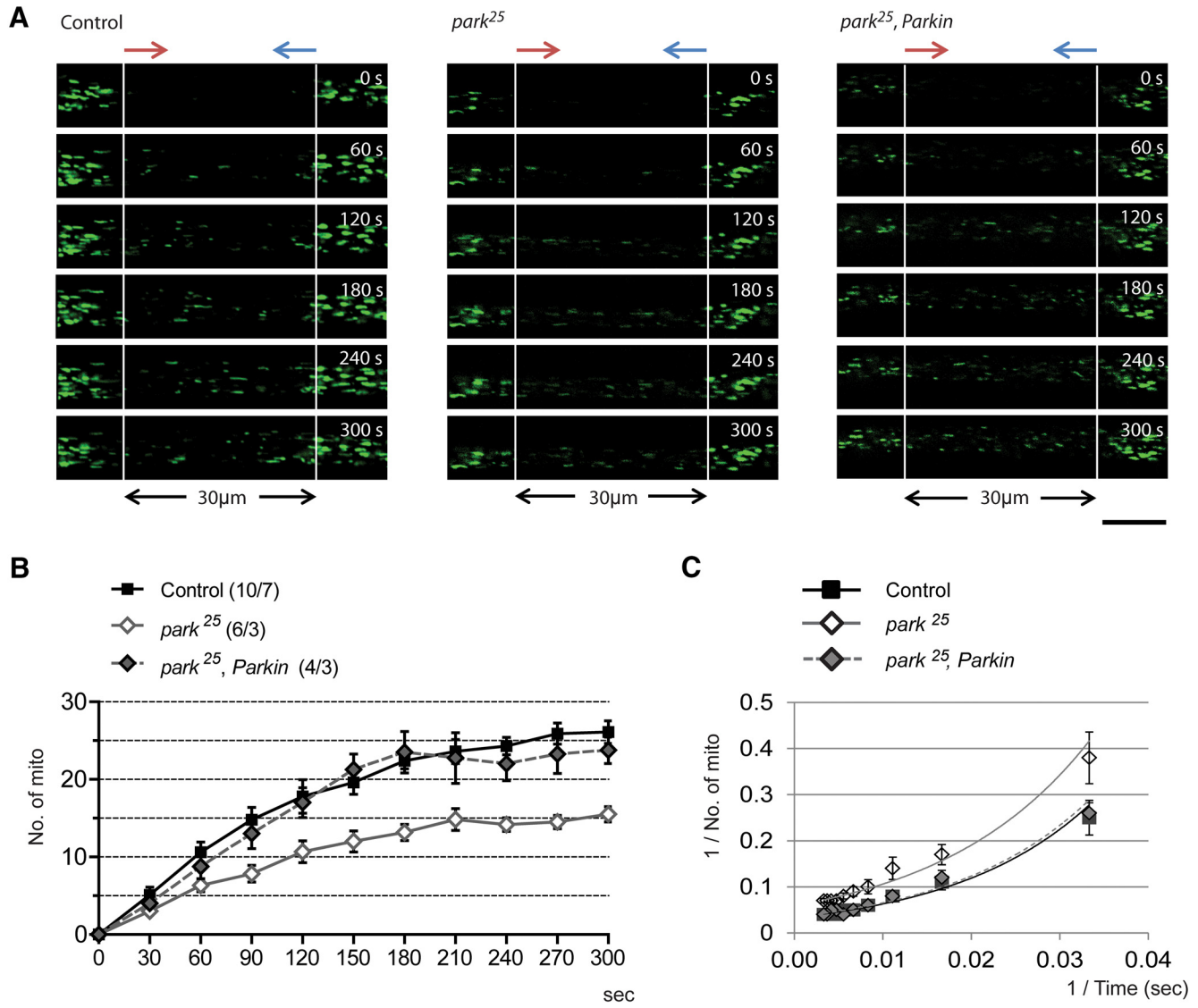

Figure 3. Reduced number of motile mitochondria is the cause of altered mitochondrial flux in *park*^{25} motor axons. ***A***, Images from 5 min time lapse of a photo-bleached region of axon in A4 SNs. The steady-state numbers of moving mitochondria are quantified by monitoring their entry into the bleached regions (30 μm). Red arrows indicate the anterograde direction, blue indicates retrograde. Scale bar, 10 μm. ***B***, Number of moving mitochondria in the bleached region reaches steady state at ~5 min. Mitochondria are counted every 30 s. ***C***, Double-reciprocal plots of the data in ***B***. The steady-state mitochondrial number is estimated from the extrapolated *y* intercepts. A total of 30 and 29 steady-state moving mitochondria are estimated in control and *park*^{25}, *Parkin* animals, while 17 steady-state moving mitochondria are estimated in *park*^{25} mutants from the 30 μm photo-bleached regions. (*n*/*n*), Number of axonal regions/number of animals. Error bars indicate the mean ± SEM.

chondria were 1.38 ± 0.03 μm in controls versus 1.28 ± 0.03 μm in *park*^{25} mutants. To determine whether a length difference in *park*^{25} mutants might be manifested not in the population average, but as a small outlying population of longer mitochondria, we examined the length distributions by a two-sample Kolmogorov–Smirnov test and found no difference between controls and *park*^{25} mutants for either moving or stationary mitochondria (data not shown). We further measured the projected area of axonal mitochondria, to confirm whether *park*^{25} mutants show any shape differences in axonal mitochondria, and found that here too *park*^{25} measurements were comparable to those for controls throughout the axons (Table 1; 0.82 ± 0.01 μm^2 with 0.56 μm mean height in controls vs 0.79 ± 0.01 μm^2 with 0.56 μm mean height in *park*^{25} mutants). Thus, Parkin seems to be dispensable for maintaining normal mitochondrial morphology in motor axons. We did not observe any correlation between morphology and motility in SN axons, so we further regressed mitochondrial velocities against their lengths to divine any relationship between the two. Although lengths were distributed from 0.35 to 4.65 μm, the net velocities of mitochondria were consistent in both directions, and there was no correlation between length and velocity or direction of movement (data not shown). Although this information seems counterintuitive on its face, it is consistent with the findings of previous studies that have shown no effect of mitochondrial length on axonal motility except at extreme, nonphysiological lengths (Amiri and Hollenbeck, 2008).

Next, we assessed the $\Delta\Psi_m$ of mitochondria from intact larval motor neurons to verify whether the sparse axonal mitochondria in *park*^{25} mutants nonetheless display the diminished membrane potential that is characteristic of senescence. TMRM was used for quantitative determination of transmembrane potential using the F_m/F_c ratio in mitochondria in thin peripheral motor nerves and NMJs adjacent to the larval A4 segment *in vivo* (Verburg and

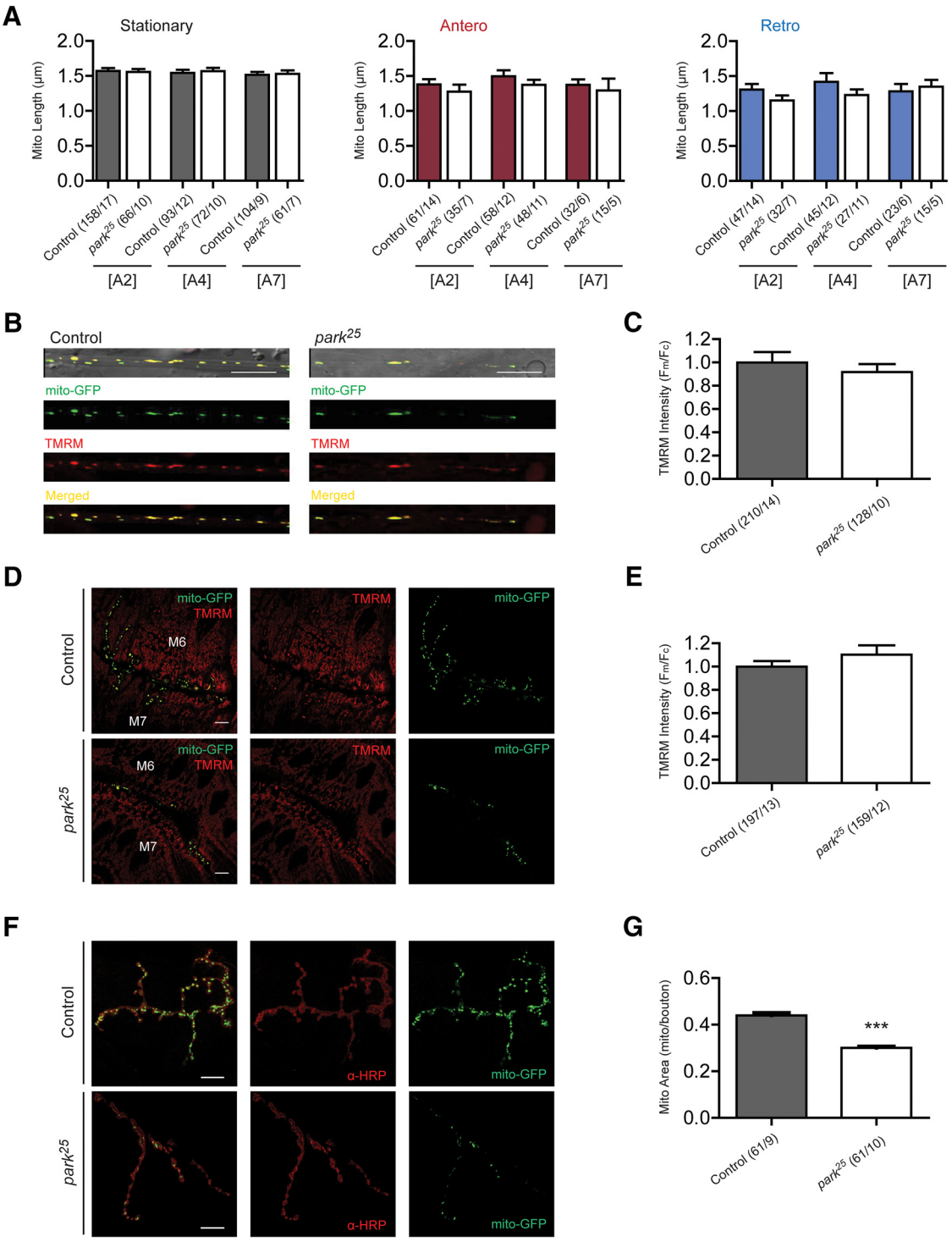

Figure 4. Parkin-deficient animals do not accumulate senescent mitochondria in motor axons and NMJs. ***A***, Mean length of axonal mitochondria in different *parkin* genotypes. Stationary and moving mitochondria are measured in axons of A2, A4, and A7 SNs. Normal mitochondrial length is preserved in *park*^{25} mutants throughout the SNs. ***B***, Representative TMRM stained images of axonal mitochondria with mito-GFP. Mitochondria are stained with TMRM (red) to indicate inner $\Delta\Psi_m$, while mito-GFP (green) reveals all axonal mitochondria. Note that mito-GFP here confirms the lower mitochondrial density in *park*^{25} axons compared with controls. Scale bars, 10 μm. ***C***, Mean F_m/F_c intensity ratio of TMRM from neurons in different *parkin* genotypes. Normal mitochondrial inner membrane potential is retained in *park*^{25} mutant axons. (*n*/*n*), Number of mitochondria/number of animals. ***D***, Representative TMRM staining images of mitochondria with mito-GFP from NMJs. NMJs are taken between muscles 7 (M7) and 6 (M6) from A4 SNs, and mitochondria in synaptic boutons are selected for $\Delta\Psi_m$ quantification. Scale bars, 10 μm. ***E***, Mean F_m/F_c intensity ratio of TMRM from NMJs in different genetic backgrounds. Normal $\Delta\Psi_m$ is retained in synaptic boutons of *park*^{25} NMJs. (*n*/*n*), Number of mitochondria/number of animals. ***F***, Images of mito-GFP (green) and anti-HRP staining (red) show mitochondria in motor synaptic boutons. Scale bars, 10 μm. ***G***, Mitochondrial density in motor NMJs. *park*^{25} mutants display reduced mitochondrial density in synaptic boutons. (*n*/*n*), Number of boutons/number of animals. Error bars indicate the mean ± SEM. Significance is determined by Student's *t* test. $^{***}p < 0.001$.

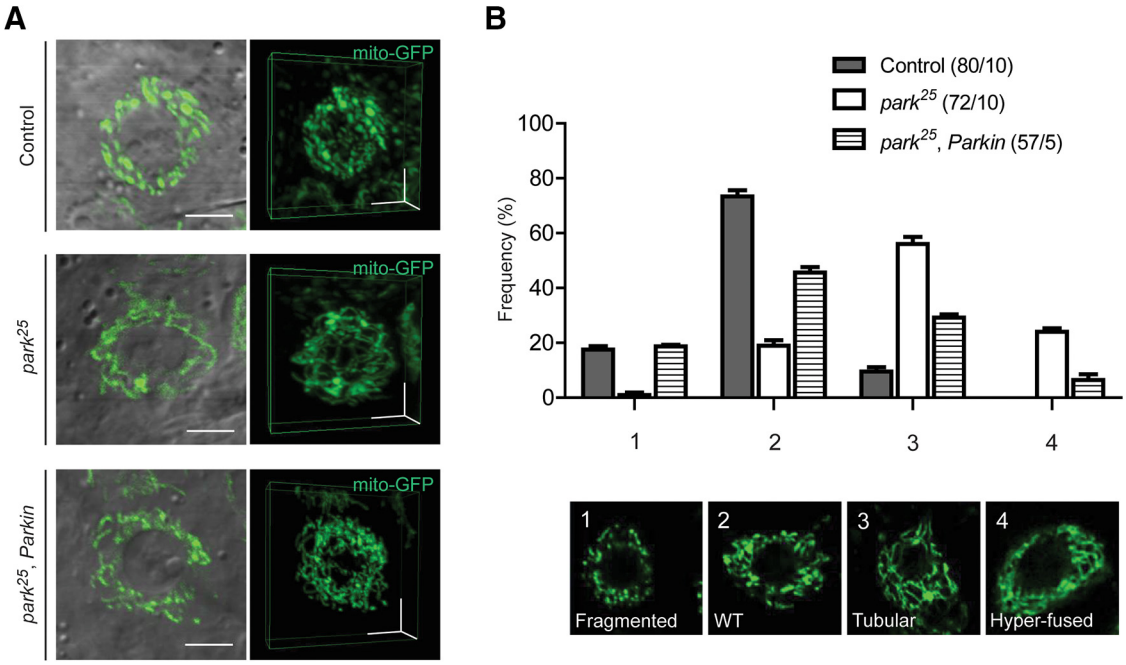

Figure 5. Parkin perturbation produces tubular, interconnected mitochondria in cell bodies. ***A***, Representative plane and three-dimensional reconstructed images of the mitochondria in motor cell bodies. Reconstructed images are generated from sections of 20 μm width (*x*), 20 μm height (*y*), and 5 μm depth (*z*) using 100 frames to construct the *z*-stacks. Scale bars, 5 μm. ***B***, Mitochondrial morphology in cell bodies of different *parkin* genotypes. Mitochondrial morphology is categorized as follows: 1, fragmented; 2, wild-type; 3, tubular; or 4, hyperfused. Tubular and hyperfused morphological defects of mitochondria are observed much more frequently in $park^{25}$ cell bodies. Morphological defects of mitochondria in $park^{25}$ cell bodies are partially restored by *UAS-Parkin* expression. (*n*/*n*), Number of cell bodies/number of animals. Data are generated in three independent analyses blinded to the genotype in the images and assessed by a two-sample Kolmogorov–Smirnov test (morphological changes of mitochondria caused by Parkin-null are significantly different from control; $D = 0.7306 >$ critical $D = 0.2209$ with a corresponding $p < 0.001$).

Hollenbeck, 2008; Shidara and Hollenbeck, 2010; Devireddy et al., 2014, 2015). Surprisingly, the $\Delta\Psi_m$ values in $park^{25}$ SNs (Fig. 4*B*,*C*) and NMJs (Fig. 4*D*,*E*) was indistinguishable from those in controls, and the reduced mitochondrial density observed in SN axons was also apparent in these thin nerves (Fig. 4*B*) and synaptic boutons (Fig. 4*F*,*G*) of $park^{25}$ mutants. Our results thus indicate that Parkin deletion fails to produce the predicted accumulation of longer and senescent mitochondria in motor axons *in vivo*; $park^{25}$ mutant animals display normal status for their axonal mitochondria.

Parkin deficit produces abnormal mitochondrial morphology in motor cell bodies

Parkin deficiency not only failed to produce the changes in axons predicted by its proposed role in mitochondrial QC—that is, an accumulation of senescent, longer mitochondria—but actually generated a dramatically reduced density of axonal mitochondria. This raised the possibility that the cell body is the locus of Parkin-dependent turnover and/or Parkin-dependent mitochondrial biogenesis, perhaps including the regulation of axonal entry. Thus, we analyzed the morphology of mitochondria in motor cell bodies of the larval nervous system; these give rise to the SN motor axons observed above. Interestingly, abnormal tubular, interconnected mitochondria were found in $park^{25}$ cell bodies (Fig. 5*A*). To quantify these complex differences in organelle morphology, we categorized the cell body mitochondria into the following four different phenotypes—fragmented (1), wild-type (2), tubular (3), and hyperfused (4)—and scored them while blinded to the genotype. Compared with controls, the $park^{25}$ cell bodies showed a much higher frequency of tubular (56% vs 9.6%) and hyperfused (24% vs 0%) mitochondria (Fig. 5*B*). Overexpression of Parkin in the $park^{25}$ mutant background largely restored normal mitochondrial morphology (Fig. 5*A*,*B*). Together with Figure 3, these data indicate that Parkin is essential for both normal mitochondrial morphology in the cell body and the entry of mitochondria into the axon, and suggest the following likely relation of the two: that normal somatic organelle morphology, reflecting a normal fission-fusion balance, is important for producing and/or launching axonal mitochondria.

Parkin-dependent mitophagy is undetectable in motor neurons *in vivo*

Studies in embryonic neurons *in vitro* have shown that autophagosomes initiate distally and undergo maturation during their retrograde transport (Maday et al., 2012; Maday and Holzbaur, 2014). Since the PINK1/Parkin pathway is thought to be necessary for local mitophagy in the distal axon (Ashrafi et al., 2014), the lack of evidence for Parkin-dependent axonal mitochondrial turnover that we found here was surprising. To probe further the role of Parkin in mitophagy *in vivo*, we visualized simultaneously mitochondria and AVs in SN motor neurons, using *D42*-driven mito-GFP and RFP-Atg8 (Barth et al., 2011). Because we had observed altered mitochondrial morphology in $park^{25}$ cell bodies, we first quantified the colocalization of AVs with mitochondria there to determine whether Parkin plays a critical role in targeting dysfunctional mitochondria for mitophagy. Consistent with our previous data, tubular and elongated mitochondria were found in $park^{25}$ cell bodies. However, mitochondria failed almost completely to colocalize with AVs in either control or $park^{25}$ cell bodies (Fig. 6*A*,*B*). Studies using *in vivo* imaging of autophagosomes in mouse Purkinje cells in the cerebellar cortex provide evidence that macroautophagy is induced by starvation (Alirezaei et al., 2010; Chen et al., 2015). Thus, to increase autophagy above basal conditions, we prevented larvae from feeding for 6 h before ob-

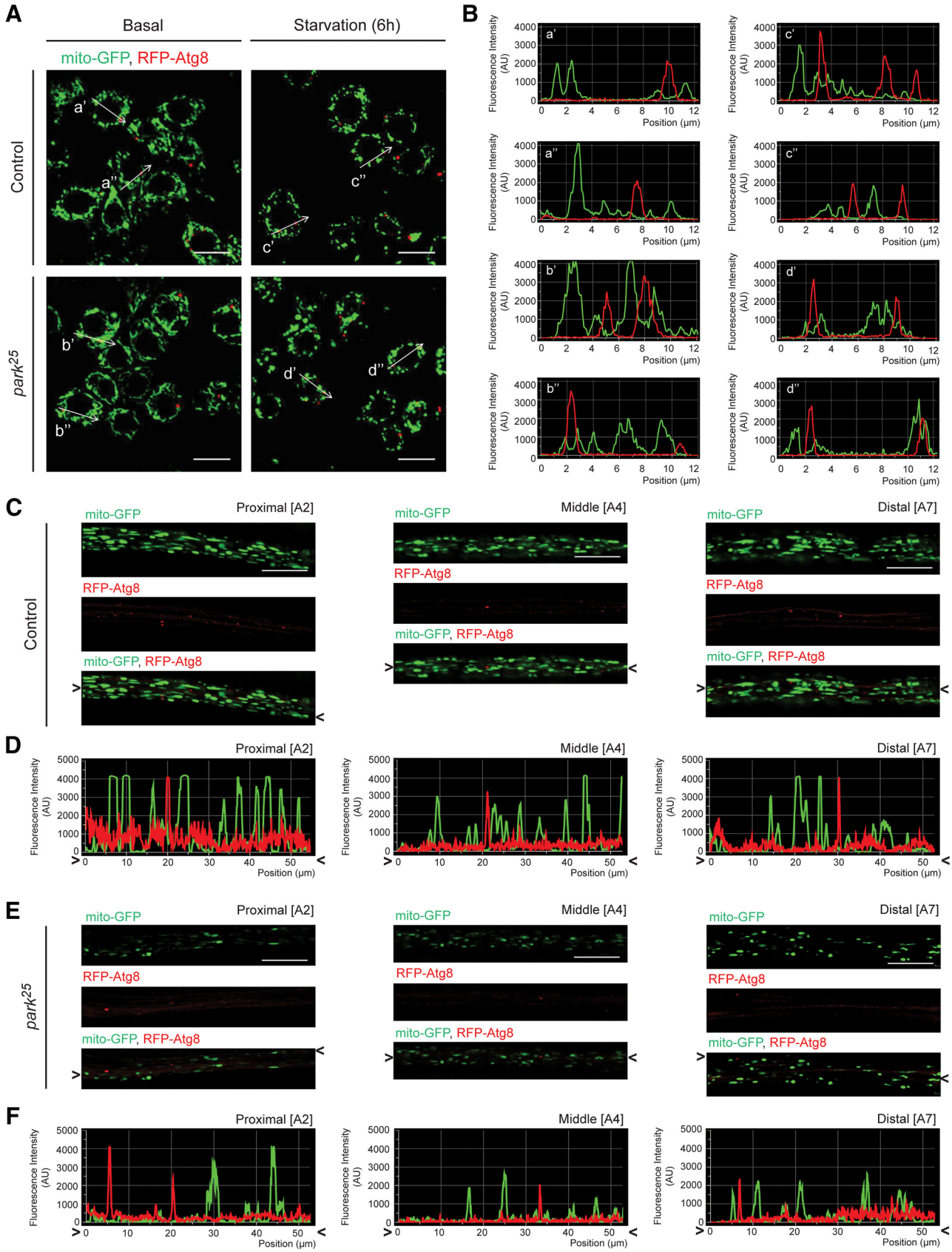

Figure 6. Mitochondria do not colocalize significantly with AVs *in vivo*. ***A***, Representative images of cell bodies in different *parkin* genotypes. mito-GFP fluorescence is used to identify mitochondria (green) and RFP-Atg8 to identify AVs (red). Autophagy is induced by 6 h of starvation. White arrows indicate lines along which organelle colocalization is analyzed for basal (***a'***, ***a''***, ***b'***, and ***b''***) and starvation (***c'***, ***c''***, ***d'***, and ***d''***) conditions. Scale bars, 10 μm. ***B***, Respective signal intensity profiles from the line scans indicate in ***A***. Distinct mito-GFP and RFP-Atg8 signals reveal no clearly detectable mitophagy events in motor cell bodies from either genotype. ***C***, Representative images of axonal mitochondria with AVs in A2, A4, and A7 SNs from control animals. Organelle colocalization is represented by oblique (A2) or rectilinear (A4 and A7) line scan analysis. Scale bars, 10 μm. ***D***, Signal intensity profiles of line scans of images in ***C***. (*Figure legend continues.*)

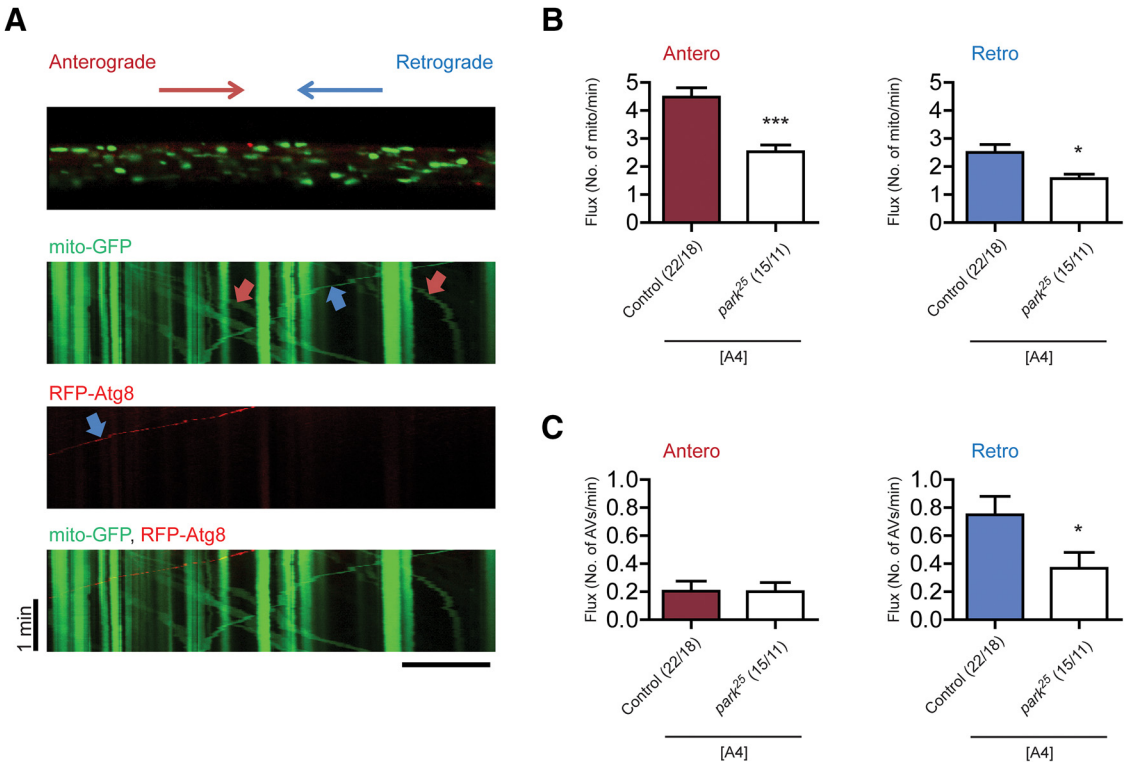

Figure 7. Parkin perturbation impairs retrograde transport of AVs. ***A***, Representative kymographs of mitochondrial and autophagosomal axonal transport from the A4 SNs axons of control animals. Red arrows indicate anterograde moving mitochondria, and blue arrows indicate retrograde moving organelles. Scale bar, 10 μm. ***B***, Mitochondrial flux in different *parkin* genotypes. ***C***, Autophagosomal flux in different *parkin* genotypes. Reduced AV flux is observed only in the retrograde direction, while reduced mitochondrial flux is observed in both directions in *park*^{25} mutant axons. (*n*/*n*), Number of axonal regions/number of animals. Error bars indicate the mean ± SEM. Significance is determined by Student's *t* test. *$p < 0.05$ and ***$p < 0.001$.

servation, triggering starvation-induced autophagy (Gomes et al., 2011; Rambold et al., 2011; Ghosh et al., 2012). Although this treatment caused mitochondrial fragmentation (Fig. 6*A*), which should render mitochondria even better candidates for engulfment, it did not generate detectable colocalization of AVs with mitochondria in either control or *park*^{25} cell bodies (Fig. 6*A*,*B*). The mito-GFP and RFP-Atg8 signals clearly represented distinct organelles in virtually every case. Thus, in cell bodies we could not test the hypothesis that Parkin deficiency would reduce the rate of mitophagy *in vivo*, because there was no detectable mitophagy even in controls, and under either normal physiological or starvation-induced autophagic conditions.

We then observed autophagosomes along motor axons to elucidate the organization of autophagy and mitophagy in that compartment. As expected from previous studies (Maday et al., 2012), axonal AVs mainly moved retrogradely and rarely changed their direction, yielding a retrograde/anterograde flux ratio of almost 4, quite distinct from the saltatory bidirectional movements of mitochondria (Fig. 7*A*). The majority of retrograde AVs displayed faster movement than mitochondria (data not shown). When we simultaneously analyzed axonal transport of mitochondria and AVs, we found that, consistent with our previous data, mitochondrial flux was diminished in both directions by Parkin deficiency (Fig. 7*B*). AV flux was also substantially reduced in *park*^{25} mutants, but specifically in the retrograde direction; *park*^{25} mutants showed anterograde AV flux equal to that of controls, while retrograde flux was reduced by 50% (Fig. 7*C*). However, as in cell bodies, in axons we observed a striking lack of colocalization of AVs with mitochondria in either control or *park*^{25} mutant animals (Fig. 6*C*–*F*). These results indicate that while AVs are obvious and their axonal transport is consistent with them having a Parkin-dependent origin and/or maturation in the distal axon, mitophagy is so rare as to be undetectable in motor neurons *in vivo*. This was true even when starvation (Fig. 6*A*,*B*) produced large numbers of small, fragmented mitochondria that are highly suitable for autophagic engulfment.

Mitophagy is common in *Drosophila* neurons *in vitro* and requires Parkin

Although we did not observe mitochondrial colocalization with AVs in *Drosophila* neurons *in vivo*, we note that most of the previous studies that have supported a role for Parkin in mitochondrial turnover and mitophagy were performed *in vitro*, with either neuronal cells (Ashrafi et al., 2014) or non-neuronal cells (Narendra et al., 2008, 2010; Matsuda et al., 2010; Lazarou et al., 2015). Thus, we examined whether autophagosomes and mitophagy can be detected in neurons *in vitro* in the same system that we used for our *in vivo* studies. We grew *Drosophila* primary motor neurons in culture, using the mito-GFP larvae as our source of cells (Bai et al., 2009; Pathak et al., 2010). In contrast to our *in vivo* results, we observed numerous AVs that colocalized with mitochondrial signals *in vitro* (Fig. 8*A*). Not only did control

←

(*Figure legend continued.*) ***E***, Representative images of axonal mitochondria with AVs in A2, A4, and A7 SNs from *park*^{25} mutant animals. Organelle colocalization is determined by oblique (A2 and A7) or rectilinear (A4) line scan analysis. Scale bars, 10 μm. ***F***, Signal intensity profiles of line scans of the images in ***E***. Mito-GFP and RFP-Atg8 signals from both genotypes show distinct, nonoverlapping distributions of mitochondria and AV signal throughout SNs. Angle brackets denote corresponding points in images (***C***, ***E***) and line scan analysis for intensity profiles (***D***, ***F***). AU, Arbitrary units.

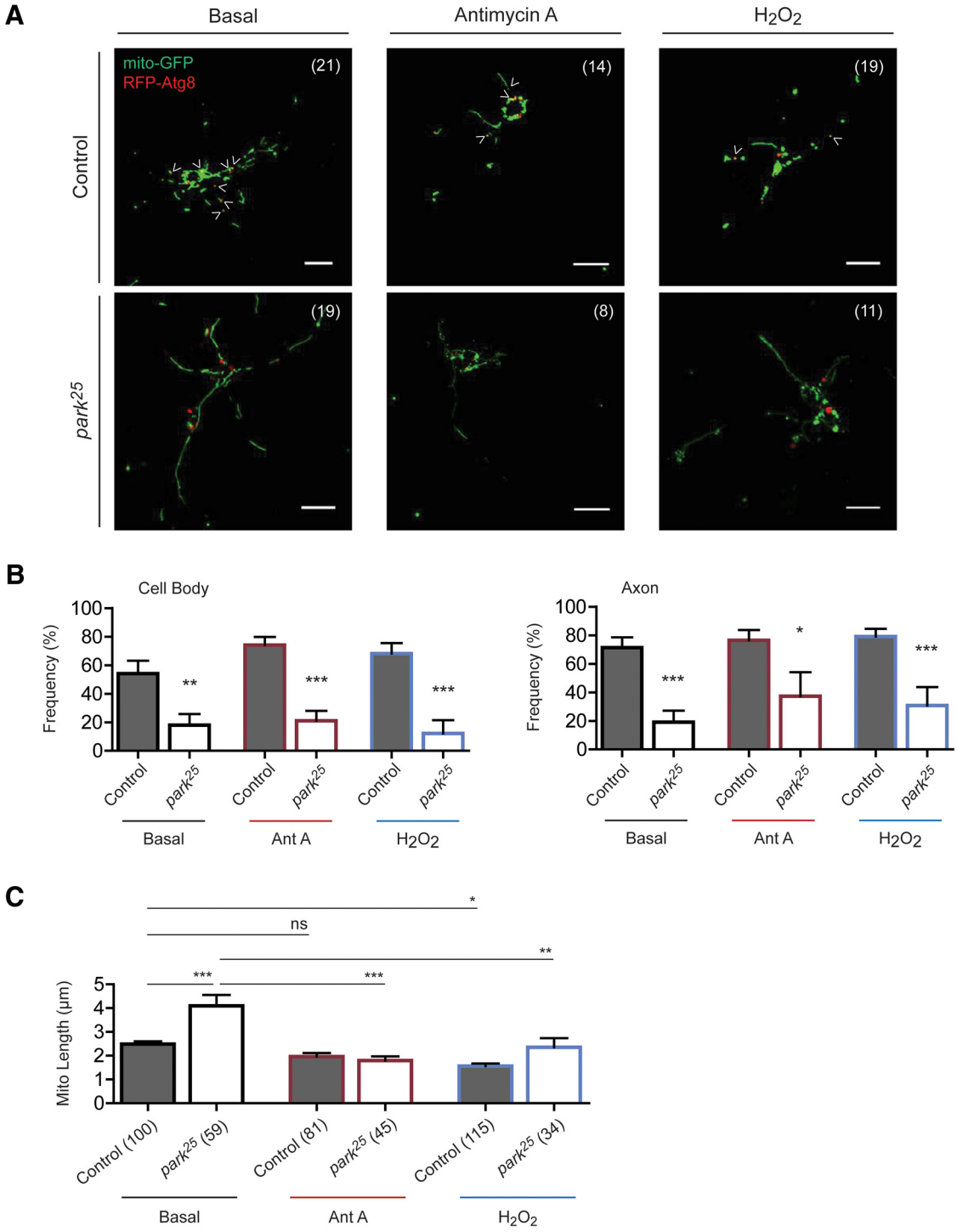

Figure 8. Parkin is essential for mitochondrial engulfment by autophagosomes *in vitro*. ***A***, Images of *in vitro* primary motor neurons expressing mito-GFP and RFP-Atg8 after 96 h in culture. For stress conditions, cells are exposed to Ant A (5 μM, 20 min) or H_2O_2 (100 μM, 1 h) before imaging. White angle brackets denote the colocalization of mitochondria with AVs. Scale bars, 10 μm. *n*, Number of cells. ***B***, Frequency of autophagosomes that contain mitochondria under each condition. Mitochondrial engulfment into AVs is inhibited in *park*^{25} mutant neurons. ***C***, Mean length of axonal mitochondria in different *parkin* genotypes in exposed conditions. *park*^{25} mutant neurons show elongated axonal mitochondria. Axonal mitochondrial elongation in *park*^{25} neurons is inhibited by either treatment (Ant A or H_2O_2). *n*, Number of mitochondria. Error bars indicate the mean ± SEM. Significance is determined by Student's *t* test (***B***) or by one-way ANOVA with Bonferroni correction (***C***). $^*p < 0.05$, $^{**}p < 0.01$, and $^{***}p < 0.001$.

neurons show this evidence for mitophagy *in vitro*, but the frequency of AV–mitochondrial colocalization was substantially reduced in neurons from *park*^{25} mutant larvae; frequencies were reduced to 33% of control levels in the cell bodies and 27% in the axons (Fig. 8*B*). This suggests that mitochondrial engulfment into autophagosomes is Parkin-dependent *in vitro*. We also observed more elongated axonal mitochondria in *park*^{25} mutant neurons *in vitro* (Fig. 8*A*,*C*), which is predicted by current models of the role of Parkin in mitochondrial turnover (Deng et al., 2008), but was not observed *in vivo*. However, the number of AVs per cell in neurons cultured from *park*^{25} mutants was not reduced relative to controls in either the cell bodies or the axons (data not

shown), arguing against Parkin control of general autophagy *in vitro*.

In neuronal (Ashrafi et al., 2014) as well as non-neuronal (Matsuda et al., 2010; Narendra et al., 2010) environments, mitochondria that undergo mitophagy mostly show an isolated, fragmented morphology. Thus, we further asked whether the size of mitochondria alone affects mitophagy, as visualized by AV–mitochondrial colocalization. To remodel mitochondria independently of Parkin perturbation, neurons were treated with 5 μM Ant A, an inhibitor of respiratory complex III that depolarizes neuronal mitochondria (Slater, 1973; Cai et al., 2012). Applying 5 μM Ant A for 20 min caused a significant decrease in mitochondrial size in *park*^{25} mutant cells (Fig. 8*C*). However, mitochondrial engulfment into autophagosomes was still inhibited in *park*^{25} mutant neurons; the frequency of AVs containing mitochondrial signal from *park*^{25} mutants was reduced to 28% of control levels in cell bodies and 49% in axons (Fig. 8*A*,*B*). In addition, we tested the role of Parkin in mitochondrial colocalization with AVs under conditions of experimental autophagic induction. Cells were treated with 100 μM H_2O_2, which induces autophagy through oxidative stress (Court and Coleman, 2012), and should promote mitophagy. Again, mitochondrial size was significantly decreased in both control and *park*^{25} mutant cells by H_2O_2 treatment for 1 h (Fig. 8*C*). However, even under conditions of oxidative stress, we saw the inhibition of mitochondrial engulfment in *park*^{25} mutant cells. In H_2O_2-treated cells, the frequency of AVs colocalizing with mitochondria was reduced to 18% of control levels in cell bodies and to 39% in axons (Fig. 8*A*,*B*). Our results suggest that Parkin regulates mitophagy *in vitro* independently of the modulation of mitochondrial size. Furthermore, since Ant A and H_2O_2 treatments cause the fragmentation of mitochondria (Fig. 8*C*) but no increase in AVs (data not shown), we also conclude that Parkin is dispensable for the remodeling of depolarized mitochondria.

Since we observed Parkin regulation of autophagosomal engulfment of mitochondria *in vitro*, we also asked whether axonal mitochondria in *park*^{25} mutant cells display normal membrane potential. The intensity ratio of TMRM staining showed that *park*^{25} mutant neurons indeed show diminished axonal $\Delta\Psi_m$ (Fig. 9*A*,*B*). Consistent with previous analysis, axonal mitochondria were also elongated in *park*^{25} mutant cells (Fig. 9*C*). Thus, we regressed mitochondrial $\Delta\Psi_m$ against their lengths to determine whether neurons *in vitro* display a key predicted consequence of Parkin-mediated QC: the accumulation of longer, less polarized mitochondria in the absence of Parkin. We found that *park*^{25} motor axons contained a small outlying population of longer mitochondria, and those mitochondria generally displayed diminished $\Delta\Psi_m$ (Fig. 9*D*,*E*). Thus, as previously reported, we too find a significant *in vitro* role for Parkin in regulating axonal mitochondrial morphology and metabolic state; however, we do not observe this mechanism in the same neurons studied *in vivo*.

Discussion

It seems likely that the cellular maintenance and long-term survival of neurons require adequate mitochondrial QC. Because neurons are highly compartmentalized cells, with structurally and functionally distinct somatodendritic and axonal compartments, it is important to understand not just whether and how dysfunctional mitochondria are turned over, but also where this occurs. In cells *in vitro*, the PINK1/Parkin pathway has been proposed both to target dysfunctional mitochondria for turnover and, in a related fashion, to regulate mitochondrial transport and dynamics. We have tested these hypotheses about Parkin-dependent mitochondrial QC in the *Drosophila* nervous system both *in vivo* and *in vitro*, and show here the following: (1) Parkin-deficient animals have dramatically reduced numbers of axonal mitochondria, but that the status and transport of these organelles remain normal; (2) the *in vivo* mitochondrial fission–fusion balance is regulated in a Parkin-dependent but somatically restricted manner; and (3) *in vivo*, mitophagy is rare in motor neurons and absent from their axons, but is both readily apparent and Parkin dependent in the same neurons *in vitro*.

Axonal transport of mitochondria has long been held to be intimately related to other organelle functions such as fission–fusion, metabolism, and turnover (Miller and Sheetz, 2004; Baloh et al., 2007; Pathak et al., 2010; Arduíno et al., 2012; Saxton and Hollenbeck, 2012). The PINK1/Parkin pathway has been proposed to coordinate mitochondrial motility with organelle turnover by specifically dissociating kinesin, the microtubule-based anterograde motor, from the organelle surface through degradation of its linker protein Miro (Wang et al., 2011). This model, however, does not explain how or why the modulation of the pathway disrupts mitochondrial movement in both the anterograde and retrograde directions. Since disruptions targeted to one direction of microtubule-based axonal transport often alter movement in both directions (Pilling et al., 2006; Park et al., 2009; Russo et al., 2009), it seems likely that the regulation of transport includes intricate coupling of both motors, kinesin and dynein. In any case, contrary to the proposed model of PINK1/Parkin dependent mitochondrial arrest, here we observed nearly unchanged mitochondrial motility behavior *in vivo* when Parkin expression was perturbed. Thus, although we found that Parkin deletion dramatically reduced mitochondrial flux in motor axons *in vivo* (Fig. 1*C*), this was derived almost entirely from a reduction in mitochondrial density to one-half that of normal axons (Figs. 2, 3), with only very modest, directionally balanced changes in motility. This is the opposite of the result expected for Parkin deletion, if this pathway were driving clearance of senescent mitochondria from the axon. It is, however, consistent with our previous demonstration that manipulation of PINK1 also fails to affect mitochondrial arrest (Devireddy et al., 2015). Since the PINK1/Parkin pathway is proposed not only to target damaged mitochondria for local turnover (Narendra et al., 2008, 2010; Matsuda et al., 2010; Ashrafi et al., 2014) but also to inhibit organelle fusion (Deng et al., 2008; Poole et al., 2010; Ziviani et al., 2010), we also expected Parkin deletion to produce elongated and metabolically compromised mitochondria *in vivo*. Surprisingly, our quantitative analyses demonstrated that mutant animals preserve both normal mitochondrial morphology and $\Delta\Psi_m$ in their axons and NMJs (Fig. 4). On the other hand, in the cell bodies of Parkin-deficient motor neurons *in vivo*, organelle morphology was dramatically altered (Fig. 5), which suggests a compartmentalized *in vivo* role for Parkin in mitochondrial QC.

What could be restricting Parkin-dependent mitochondrial QC to cell bodies *in vivo*? One possibility is the dynamic interplay with other organelles, such as endoplasmic reticulum (ER). ER tubules form membrane contact sites with a number of other organelles (Rowland and Voeltz, 2012; Rowland et al., 2014), and such contacts regulate diverse neuronal functions, including motor protein-dependent organelle transport and neurite outgrowth (Raiborg et al., 2015). Recently, it has been proposed that ER tubules also play a regulatory role in mitochondrial division by contacting mitochondria and causing their constriction before the recruitment of the mitochondrial fission protein Drp1 (Friedman et al., 2011). Although ER elements are found in the axon and contribute to the transport and distribution of axonal

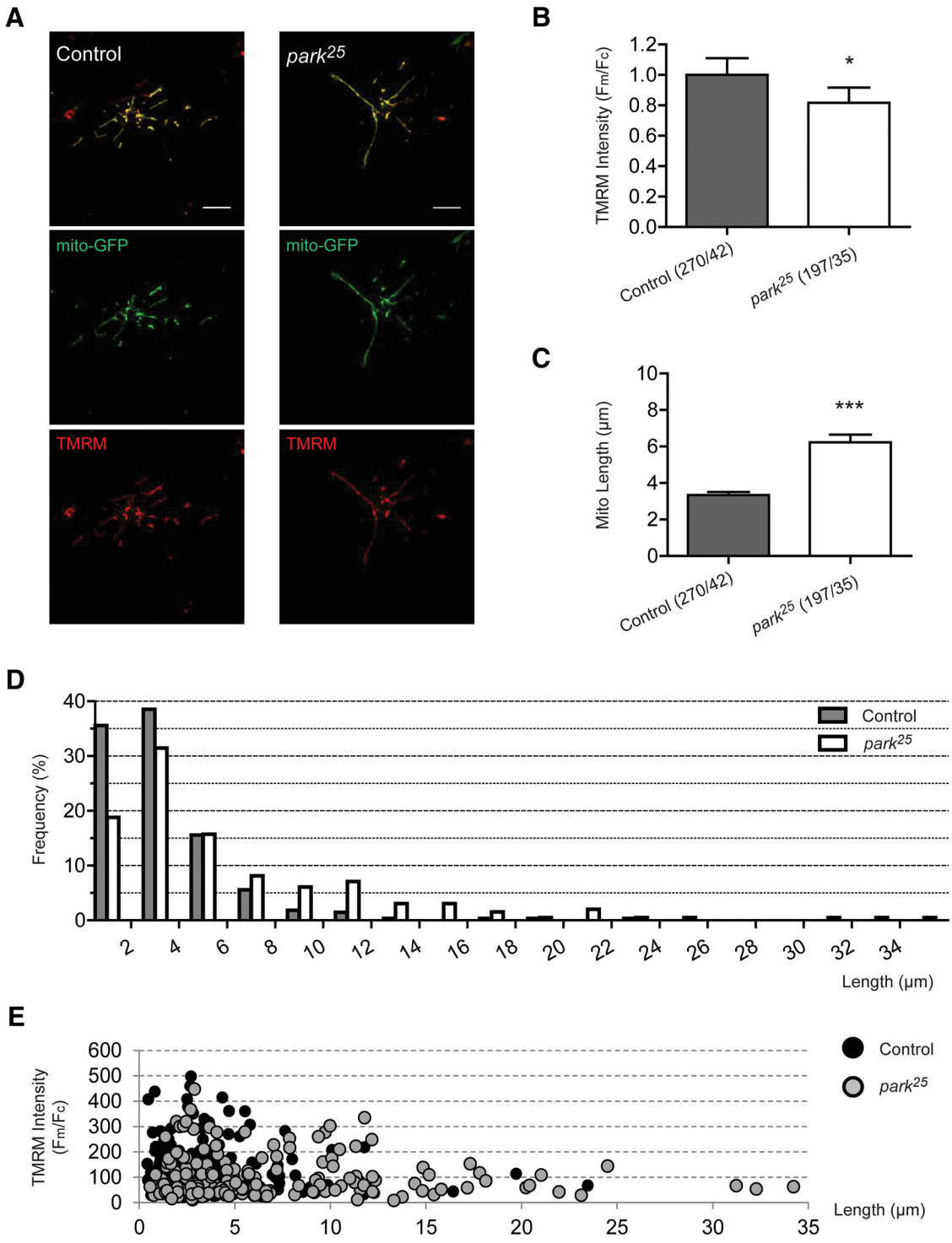

Figure 9. Parkin perturbation produced elongated mitochondria with diminished mitochondrial $\Delta\Psi_m$ *in vitro*. ***A***, Representative images of motor neurons stained with TMRM *in vitro* after 96 h in culture. Scale bars, 10 μm. ***B***, Mean F_m/F_c intensity ratio of TMRM from cultured neurons of different *parkin* genotypes. ***C***, Mean length of axonal mitochondria *in vitro*. ***D***, Length distribution of axonal mitochondria *in vitro*. ***E***, Relationship between mitochondrial $\Delta\Psi_m$ and length in axons *in vitro*. Correlation coefficients: control ($R^2 = 0.0049$) and *park*^{25} ($R^2 = 0.0004$). *park*^{25} mutant neurons *in vitro* show decreased $\Delta\Psi_m$ and elongated axonal mitochondria. (*n*/*n*), Number of mitochondria/number of cells. Error bars indicate the mean ± SEM. Significance is determined by Student's *t* test (***B***, ***C***; *$p < 0.05$ and ***$p < 0.001$) or by two-sample Kolmogorov–Smirnov test (***D***; K–S statistics show significant difference; $D = 0.2107 >$ critical $D = 0.1274$ with a corresponding $p < 0.001$).

cargos (González and Couve, 2014), ER tubules apparently maintain their contact sites with other organelles independent of microtubules (Rowland et al., 2014), and their major network is located in the cell body (Berridge, 1998; Verkhratsky and Petersen, 1998). Thus, it is plausible that the role of ER in mitochondrial morphology restricts the compartmental localization of the defects caused by Parkin perturbation *in vivo*. In addition, if the somatic compartment is the main site of mitochondrial turnover (Safiulina and Kaasik, 2013), then the entry of mitochondria into the axon from the cell body, and perhaps their subsequent return,

are critically important in regulating the neuronal mitochondrial life cycle. In this context, we propose that mature neurons possess a QC barrier between the cell body and the axon that restricts axonal entry to those mitochondria of appropriate size, morphology, and metabolic status. This proposal is consistent with recent evidence that the preaxonal exclusion zone in the hillock provides a cytoplasmic boundary for the entry of vesicles into the axonal domain (Farías et al., 2015). Thus, the disruption of the fission–fusion balance in cell bodies by Parkin perturbation, which caused abnormal, interconnected mitochondria in the cell body, may physically disrupt the "launching process" of dysfunctional organelles into the axon.

If new mitochondria to supply the axon are generated largely in the cell body *in vivo*, then the importance of axonal transport looms even larger, especially anterograde movement. Indeed, it is notable that the same reduced-axonal-density phenotype that we observed has previously been reported in motor axons of *Drosophila* SNs with disrupted motor protein expression (Pilling et al., 2006). In that study, it was remarkable that only kinesin heavy chain mutants displayed reduced mitochondrial density in SNs, while mutations in *dynein* retained the normal compliment of axonal mitochondria. Furthermore, our previous report demonstrated that Parkin selectively restored the abnormal mitochondria of *PINK1* mutants only in cell bodies, not in axons (Devireddy et al., 2015). In addition, it is noteworthy that a previous study (Cai et al., 2012) of cultured cortical neurons *in vitro* shows the restricted Parkin-mediated mitophagy only in the somatodendritic compartment. Together, these findings suggest a compartmentalized *in vivo* role of PINK1/Parkin in neuronal mitochondrial turnover and provide further evidence that the mitochondrial supply from the cell body is critically important for preserving organelle numbers and distribution in axons.

We did observe the morphological remodeling of mitochondria under stress conditions both *in vivo* and *in vitro*: starvation *in vivo* (Fig. 6*A*), as well as Ant A and H_2O_2 treatments *in vitro* (Fig. 8*C*) both produced fragmented mitochondria, even in the absence of Parkin. It is possible that mitochondrial fission is regulated independently of Parkin and/or upregulated by stress conditions. However, we observed several dramatic distinctions in the mitochondrial life cycle between motor neurons *in vivo* and *in vitro*. First, we rarely observed AVs that colocalized with mitochondria anywhere in motor neurons *in vivo*, whereas Parkin-dependent mitophagy was obvious in the same neurons *in vitro*. Second, axonal mitochondria under Parkin perturbation were elongated and displayed diminished $\Delta\Psi_m$ in motor neurons *in vitro*, but had virtually normal status *in vivo*. Thus, while our observations from *in vitro* neurons supported the current models for the role of Parkin in axonal mitochondrial QC, targeting senescent mitochondria and promoting mitochondrial fission, data from the same neurons *in vivo* expressly did not.

What could explain these differences? One possibility is that fully connected neurons *in vivo* have established a physical filter for mitochondria between the cell body and axon that remains less developed *in vitro*. In support of this idea, we noted that the most axonal mitochondria *in vivo* were morphologically nearly uniform and approximately two times shorter than axonal mitochondria in cultured neurons (Figs. 4*A*, 9*C*). In addition, axonal mitochondria *in vitro* often extended continuously from the cell body into the axon (Fig. 8*A*), a feature that is rarely, if ever, seen *in vivo*, suggesting that the filter between the cell body and axon is absent or more permissive in cultured neurons. If mitochondrial entry into the axon is more restricted *in vivo* than *in vitro*, it could also explain the greatly downregulated axonal mitophagy that we observed *in vivo*. It is also important to note that mature neurons *in vivo* are functionally associated with surrounding cells and tissues. Recent evidence from mouse optic nerve head *in vivo* (Davis et al., 2014) shows the extrusion and transcellular degradation of axonal mitochondria, "transmitophagy," a process that could provide a different avenue for mitochondrial turnover in the periphery, and could contribute to the lack of axonal mitophagy observed *in vivo*. It is also likely that neurons *in vitro*, subjected to hyperoxic conditions, are more susceptible to environmental stress. Thus, they may upregulate their mechanisms for mitochondrial clearance.

In summary, comparing *Drosophila* motor neurons *in vivo* and *in vitro*, we find a dramatic difference that indicates a highly compartmentalized *in vivo* role for Parkin in mitochondrial QC. Unlike *in vitro* conditions, the *in vivo* role of Parkin does not appear obviously related to mitophagy, and is restricted to the cell body where it seems to modulate mitochondrial fission–fusion balance and, indirectly, the mitochondrial composition of the axon. Our results re-emphasize the intricate interdependence of mitochondrial dynamics and axonal transport, and suggest that neuronal mitochondrial QC occurs in the cell body, and that a critical step is the initial access of mitochondria to the axon after organelle biogenesis.

References

Alirezaei M, Kemball CC, Flynn CT, Wood MR, Whitton JL, Kiosses WB (2010) Short-term fasting induces profound neuronal autophagy. Autophagy 6:702–710. CrossRef Medline

Amiri M, Hollenbeck PJ (2008) Mitochondrial biogenesis in the axons of vertebrate peripheral neurons. Dev Neurobiol 68:1348–1361. CrossRef Medline

Arduíno DM, Esteves AR, Cortes L, Silva DF, Patel B, Grazina M, Swerdlow RH, Oliveira CR, Cardoso SM (2012) Mitochondrial metabolism in Parkinson's disease impairs quality control autophagy by hampering microtubule-dependent traffic. Hum Mol Genet 21:4680–4702. CrossRef Medline

Ashrafi G, Schlehe JS, LaVoie MJ, Schwarz TL (2014) Mitophagy of damaged mitochondria occurs locally in distal neuronal axons and requires PINK1 and Parkin. J Cell Biol 206:655–670. CrossRef Medline

Bai J, Sepp KJ, Perrimon N (2009) Culture of Drosophila primary cells dissociated from gastrula embryos and their use in RNAi screening. Nat Protoc 4:1502–1512. CrossRef Medline

Baloh RH, Schmidt RE, Pestronk A, Milbrandt J (2007) Altered axonal mitochondrial transport in the pathogenesis of Charcot-Marie-Tooth disease from mitofusin 2 mutations. J Neurosci 27:422–430. CrossRef Medline

Barth JM, Szabad J, Hafen E, Köhler K (2011) Autophagy in Drosophila ovaries is induced by starvation and is required for oogenesis. Cell Death Differ 18:915–924. CrossRef Medline

Berridge MJ (1998) Neuronal calcium signaling. Neuron 21:13–26. CrossRef Medline

Cagalinec M, Safiulina D, Liiv M, Liiv J, Choubey V, Wareski P, Veksler V, Kaasik A (2013) Principles of the mitochondrial fusion and fission cycle in neurons. J Cell Sci 126:2187–2197. CrossRef Medline

Cai Q, Zakaria HM, Simone A, Sheng ZH (2012) Spatial parkin translocation and degradation of damaged mitochondria via mitophagy in live cortical neurons. Curr Biol 22:545–552. CrossRef Medline

Chan DC (2006) Mitochondrial fusion and fission in mammals. Annu Rev Cell Dev Biol 22:79–99. CrossRef Medline

Chen H, Chan DC (2009) Mitochondrial dynamics—fusion, fission, movement, and mitophagy—in neurodegenerative diseases. Hum Mol Genet 18:R169–R176. CrossRef Medline

Chen X, Kondo K, Motoki K, Homma H, Okazawa H (2015) Fasting activates macroautophagy in neurons of Alzheimer's disease mouse model but is insufficient to degrade amyloid-beta. Sci Rep 5:12115. CrossRef Medline

Court FA, Coleman MP (2012) Mitochondria as a central sensor for axonal degenerative stimuli. Trends Neurosci 35:364–372. CrossRef Medline

Davis AF, Clayton DA (1996) In situ localization of mitochondrial DNA

replication in intact mammalian cells. J Cell Biol 135:883–893. CrossRef Medline

Davis CH, Kim KY, Bushong EA, Mills EA, Boassa D, Shih T, Kinebuchi M, Phan S, Zhou Y, Bihlmeyer NA, Nguyen JV, Jin Y, Ellisman MH, Marsh-Armstrong N (2014) Transcellular degradation of axonal mitochondria. Proc Natl Acad Sci U S A 111:9633–9638. CrossRef Medline

Deinhardt K, Salinas S, Verastegui C, Watson R, Worth D, Hanrahan S, Bucci C, Schiavo G (2006) Rab5 and Rab7 control endocytic sorting along the axonal retrograde transport pathway. Neuron 52:293–305. CrossRef Medline

Deng H, Dodson MW, Huang H, Guo M (2008) The Parkinson's disease genes pink1 and parkin promote mitochondrial fission and/or inhibit fusion in Drosophila. Proc Natl Acad Sci U S A 105:14503–14508. CrossRef Medline

Devireddy S, Sung H, Liao PC, Garland-Kuntz E, Hollenbeck PJ (2014) Analysis of mitochondrial traffic in Drosophila. Methods Enzymol 547: 131–150. CrossRef Medline

Devireddy S, Liu A, Lampe T, Hollenbeck PJ (2015) The organization of mitochondrial quality control and life cycle in the nervous system *in vivo* in the absence of PINK1. J Neurosci 35:9391–9401. CrossRef Medline

Fang Y, Soares L, Teng X, Geary M, Bonini NM (2012) A novel Drosophila model of nerve injury reveals an essential role of Nmnat in maintaining axonal integrity. Curr Biol 22:590–595. CrossRef Medline

Fang Y, Soares L, Bonini NM (2013) Design and implementation of in vivo imaging of neural injury responses in the adult Drosophila wing. Nat Protoc 8:810–819. CrossRef Medline

Farías GG, Guardia CM, Britt DJ, Guo X, Bonifacino JS (2015) Sorting of dendritic and axonal vesicles at the pre-axonal exclusion zone. Cell Rep 13:1221–1232. CrossRef Medline

Friedman JR, Lackner LL, West M, DiBenedetto JR, Nunnari J, Voeltz GK (2011) ER tubules mark sites of mitochondrial division. Science 334: 358–362. CrossRef Medline

Ghosh D, Walton JL, Roepe PD, Sinai AP (2012) Autophagy is a cell death mechanism in Toxoplasma gondii. Cell Microbiol 14:589–607. CrossRef Medline

Glater EE, Megeath LJ, Stowers RS, Schwarz TL (2006) Axonal transport of mitochondria requires milton to recruit kinesin heavy chain and is light chain independent. J Cell Biol 173:545–557. CrossRef Medline

Gomes LC, Di Benedetto G, Scorrano L (2011) During autophagy mitochondria elongate, are spared from degradation and sustain cell viability. Nat Cell Biol 13:589–598. CrossRef Medline

González C, Couve A (2014) The axonal endoplasmic reticulum and protein trafficking: cellular bootlegging south of the soma. Semin Cell Dev Biol 27:23–31. CrossRef Medline

Greene JC, Whitworth AJ, Kuo I, Andrews LA, Feany MB, Pallanck LJ (2003) Mitochondrial pathology and apoptotic muscle degeneration in Drosophila parkin mutants. Proc Natl Acad Sci U S A 100:4078–4083. CrossRef Medline

Guo X, Macleod GT, Wellington A, Hu F, Panchumarthi S, Schoenfield M, Marin L, Charlton MP, Atwood HL, Zinsmaier KE (2005) The GTPase dMiro is required for axonal transport of mitochondria to Drosophila synapses. Neuron 47:379–393. CrossRef Medline

Hirokawa N, Niwa S, Tanaka Y (2010) Molecular motors in neurons: transport mechanisms and roles in brain function, development, and disease. Neuron 68:610–638. CrossRef Medline

Lazarou M, Sliter DA, Kane LA, Sarraf SA, Wang C, Burman JL, Sideris DP, Fogel AI, Youle RJ (2015) The ubiquitin kinase PINK1 recruits autophagy receptors to induce mitophagy. Nature 524:309–314. CrossRef Medline

Liu S, Sawada T, Lee S, Yu W, Silverio G, Alapatt P, Millan I, Shen A, Saxton W, Kanao T, Takahashi R, Hattori N, Imai Y, Lu B (2012) Parkinson's disease-associated kinase PINK1 regulates Miro protein level and axonal transport of mitochondria. PLoS Genet 8:e1002537. CrossRef Medline

Louie K, Russo GJ, Salkoff DB, Wellington A, Zinsmaier KE (2008) Effects of imaging conditions on mitochondrial transport and length in larval motor axons of Drosophila. Comp Biochem Physiol A Mol Integr Physiol 151:159–172. CrossRef Medline

Maday S, Holzbaur EL (2014) Autophagosome biogenesis in primary neurons follows an ordered and spatially regulated pathway. Dev Cell 30:71–85. CrossRef Medline

Maday S, Wallace KE, Holzbaur EL (2012) Autophagosomes initiate distally and mature during transport toward the cell soma in primary neurons. J Cell Biol 196:407–417. CrossRef Medline

Matsuda N, Sato S, Shiba K, Okatsu K, Saisho K, Gautier CA, Sou YS, Saiki S, Kawajiri S, Sato F, Kimura M, Komatsu M, Hattori N, Tanaka K (2010) PINK1 stabilized by mitochondrial depolarization recruits Parkin to damaged mitochondria and activates latent Parkin for mitophagy. J Cell Biol 189:211–221. CrossRef Medline

Miller KE, Sheetz MP (2004) Axonal mitochondrial transport and potential are correlated. J Cell Sci 117:2791–2804. CrossRef Medline

Misko A, Jiang S, Wegorzewska I, Milbrandt J, Baloh RH (2010) Mitofusin 2 is necessary for transport of axonal mitochondria and interacts with the Miro/Milton complex. J Neurosci 30:4232–4240. CrossRef Medline

Moughamian AJ, Holzbaur EL (2012) Dynactin is required for transport initiation from the distal axon. Neuron 74:331–343. CrossRef Medline

Narendra D, Tanaka A, Suen DF, Youle RJ (2008) Parkin is recruited selectively to impaired mitochondria and promotes their autophagy. J Cell Biol 183:795–803. CrossRef Medline

Narendra DP, Jin SM, Tanaka A, Suen DF, Gautier CA, Shen J, Cookson MR, Youle RJ (2010) PINK1 is selectively stabilized on impaired mitochondria to activate Parkin. PLoS Biol 8:e1000298. CrossRef Medline

Okamoto K, Shaw JM (2005) Mitochondrial morphology and dynamics in yeast and multicellular eukaryotes. Annu Rev Genet 39:503–536. CrossRef Medline

Park JJ, Koshimizu H, Loh YP (2009) Biogenesis and transport of secretory granules to release site in neuroendocrine cells. J Mol Neurosci 37:151–159. CrossRef Medline

Pathak D, Sepp KJ, Hollenbeck PJ (2010) Evidence that myosin activity opposes microtubule-based axonal transport of mitochondria. J Neurosci 30:8984–8992. CrossRef Medline

Pilling AD, Horiuchi D, Lively CM, Saxton WM (2006) Kinesin-1 and Dynein are the primary motors for fast transport of mitochondria in Drosophila motor axons. Mol Biol Cell 17:2057–2068. CrossRef Medline

Poole AC, Thomas RE, Andrews LA, McBride HM, Whitworth AJ, Pallanck LJ (2008) The PINK1/Parkin pathway regulates mitochondrial morphology. Proc Natl Acad Sci U S A 105:1638–1643. CrossRef Medline

Poole AC, Thomas RE, Yu S, Vincow ES, Pallanck L (2010) The mitochondrial fusion-promoting factor mitofusin is a substrate of the PINK1/parkin pathway. PLoS One 5:e10054. CrossRef Medline

Raiborg C, Wenzel EM, Pedersen NM, Olsvik H, Schink KO, Schultz SW, Vietri M, Nisi V, Bucci C, Brech A, Johansen T, Stenmark H (2015) Repeated ER-endosome contacts promote endosome translocation and neurite outgrowth. Nature 520:234–238. CrossRef Medline

Rambold AS, Kostelecky B, Elia N, Lippincott-Schwartz J (2011) Tubular network formation protects mitochondria from autophagosomal degradation during nutrient starvation. Proc Natl Acad Sci U S A 108:10190–10195. CrossRef Medline

Reis K, Fransson A, Aspenström P (2009) The Miro GTPases: at the heart of the mitochondrial transport machinery. FEBS Lett 583:1391–1398. CrossRef Medline

Rowland AA, Voeltz GK (2012) Endoplasmic reticulum-mitochondria contacts: function of the junction. Nat Rev Mol Cell Biol 13:607–625. CrossRef Medline

Rowland AA, Chitwood PJ, Phillips MJ, Voeltz GK (2014) ER contact sites define the position and timing of endosome fission. Cell 159:1027–1041. CrossRef Medline

Rugarli EI, Langer T (2012) Mitochondrial quality control: a matter of life and death for neurons. EMBO J 31:1336–1349. CrossRef Medline

Russo GJ, Louie K, Wellington A, Macleod GT, Hu F, Panchumarthi S, Zinsmaier KE (2009) *Drosophila* Miro is required for both anterograde and retrograde axonal mitochondrial transport. J Neurosci 29:5443–5455. CrossRef Medline

Safiulina D, Kaasik A (2013) Energetic and dynamic: how mitochondria meet neuronal energy demands. PLoS Biol 11:e1001755. CrossRef Medline

Saxton WM, Hollenbeck PJ (2012) The axonal transport of mitochondria. J Cell Sci 125:2095–2104. CrossRef Medline

Shidara Y, Hollenbeck PJ (2010) Defects in mitochondrial axonal transport and membrane potential without increased reactive oxygen species production in a *Drosophila* model of Friedreich ataxia. J Neurosci 30:11369–11378. CrossRef Medline

Slater EC (1973) The mechanism of action of the respiratory inhibitor, antimycin. Biochim Biophys Acta 301:129–154. CrossRef Medline

Song Z, Ghochani M, McCaffery JM, Frey TG, Chan DC (2009) Mitofusins and OPA1 mediate sequential steps in mitochondrial membrane fusion. Mol Biol Cell 20:3525–3532. CrossRef Medline

Stowers RS, Megeath LJ, Górska-Andrzejak J, Meinertzhagen IA, Schwarz TL (2002) Axonal transport of mitochondria to synapses depends on milton, a novel Drosophila protein. Neuron 36:1063–1077. CrossRef Medline

Verburg J, Hollenbeck PJ (2008) Mitochondrial membrane potential in axons increases with local nerve growth factor or semaphorin signaling. J Neurosci 28:8306–8315. CrossRef Medline

Verkhratsky AJ, Petersen OH (1998) Neuronal calcium stores. Cell Calcium 24:333–343. CrossRef Medline

Verstreken P, Ly CV, Venken KJ, Koh TW, Zhou Y, Bellen HJ (2005) Synaptic mitochondria are critical for mobilization of reserve pool vesicles at Drosophila neuromuscular junctions. Neuron 47:365–378. CrossRef Medline

Wang X, Winter D, Ashrafi G, Schlehe J, Wong YL, Selkoe D, Rice S, Steen J, LaVoie MJ, Schwarz TL (2011) PINK1 and Parkin target Miro for phosphorylation and degradation to arrest mitochondrial motility. Cell 147:893–906. CrossRef Medline

Yu Y, Lee HC, Chen KC, Suhan J, Qiu M, Ba Q, Yang G (2016) Inner membrane fusion mediates spatial distribution of axonal mitochondria. Sci Rep 6:18981. CrossRef Medline

Ziviani E, Tao RN, Whitworth AJ (2010) Drosophila parkin requires PINK1 for mitochondrial translocation and ubiquitinates mitofusin. Proc Natl Acad Sci U S A 107:5018–5023. CrossRef Medline